OVERSAMPLED DISTORTION-AWARE PRECODING WITH EFFICIENT OOB RADIATION CONTROL FOR QUANTIZED MASSIVE MIMO AND PERFORMANCE ANALYSIS

A THESIS SUBMITTED TO
THE GRADUATE SCHOOL OF NATURAL AND APPLIED SCIENCES
OF
MIDDLE EAST TECHNICAL UNIVERSITY

BY

YUSUF KARABACAKOĞLU

IN PARTIAL FULFILLMENT OF THE REQUIREMENTS
FOR
THE DEGREE OF MASTER OF SCIENCE
IN
ELECTRICAL AND ELECTRONICS ENGINEERING

AUGUST 2023

Approval of the thesis:

OVERSAMPLED DISTORTION-AWARE PRECODING WITH EFFICIENT OOB RADIATION CONTROL FOR QUANTIZED MASSIVE MIMO AND PERFORMANCE ANALYSIS

submitted by YUSUF KARABACAKOĞLU in partial fulfillment of the requirements for the degree of **Master of Science in Electrical and Electronics Engineering Department, Middle East Technical University** by,

Prof. Dr. Halil Kalıpçılar
Dean, Graduate School of **Natural and Applied Sciences** _____

Prof. Dr. İlkay Ulusoy
Head of Department, **Electrical and Electronics Engineering** _____

Assist. Prof. Dr. Gökhan Muzaffer Güvensen
Supervisor, **Electrical and Electronics Engineering, METU** _____

Examining Committee Members:

Prof. Dr. Ali Özgür Yılmaz
Electrical and Electronics Engineering, METU _____

Assist. Prof. Dr. Gökhan Muzaffer Güvensen
Electrical and Electronics Engineering, METU _____

Prof. Dr. Emre Aktaş
Electrical and Electronics Engineering, Hacettepe University _____

Date:25.08.2023

I hereby declare that all information in this document has been obtained and presented in accordance with academic rules and ethical conduct. I also declare that, as required by these rules and conduct, I have fully cited and referenced all material and results that are not original to this work.

Name, Surname: Yusuf Karabacakoğlu

Signature :

ABSTRACT

OVERSAMPLED DISTORTION-AWARE PRECODING WITH EFFICIENT OOB RADIATION CONTROL FOR QUANTIZED MASSIVE MIMO AND PERFORMANCE ANALYSIS

Yusuf Karabacakoğlu,
M.S., Department of Electrical and Electronics Engineering
Supervisor: Assist. Prof. Dr. Gökhan Muzaffer Güvensen

August 2023, 56 pages

In this study, the nonlinear effects of the quantization due to low-resolution digital-to-analog converters (DACs) will be investigated. Massive multiple-input multiple-output (MIMO) systems have received significant attention in academia and industry due to their remarkable advantages in terms of spectral and energy efficiency. However, the deployment of large number of antennas and circuitry required for generating transmit signals at the base station (BS) can be expensive and power-consuming. To address this, various studies in the literature proposes a practical solution by utilizing cheaper and power-efficient hardware, with a specific focus on the DACs used in the RF chain. By employing a pair of low-resolution DACs at each antenna of the massive MIMO array, both the cost and power consumption can be reduced, making it favorable for such systems. However, the use of low-resolution DACs introduces quantization distortion, which can severely affect system performance. To mitigate this distortion, various quantized precoding algorithms have been proposed in the literature. This study presents an iterative distortion-aware precoder that works with oversampling DACs, which have a sampling rate higher than the symbol rate, since oversampling is an effective approach for reducing quantization distortion in massive

MIMO systems. We demonstrate that the precoder we propose outperforms the existing oversampling precoders of comparable computational complexity in the literature by efficiently maximizing the in-band error-rate performance while minimizing out-of-band emissions. Furthermore, we perform a performance analysis of the proposed precoder and quantized zero-forcing (ZF) precoder for various scenarios, including multiple base stations in adjacent channel bands and aliasing.

Keywords: Iterative precoder, quantization, 1-bit digital-to-analog converter (DAC), massive MIMO, oversampling, upsampling, multi-bit, wideband, frequency-selective channel, downlink, zero-forcing.

ÖZ

NİCEMLEME VE AŞIRI ÖRNEKLEME ALTINDA ÇALIŞABİLEN BOZULMAYA DUYARLI OOB EMİSYON KONTROLLÜ BİR GENİŞ-BANT KİTLESEL MIMO ÖN-KODLAYICI VE PERFORMANS ANALİZİ

Yusuf Karabacakoğlu,
Yüksek Lisans, Elektrik ve Elektronik Mühendisliği Bölümü
Tez Yöneticisi: Dr. Öğr. Üyesi. Gökhan Muzaffer Güvensen

Ağustos 2023 , 56 sayfa

Bu çalışmada düşük çözünürlüklü dijital-analog dönüştürücülerin (DAC) doğrusal olmayan etkileri araştırılmıştır. Kitlesel çoklu-girdili-çoklu-çıktılı (MIMO) sistemler sahip oldukları spektral ve enerji verimliliğinden dolayı akademi ve endüstride oldukça dikkat çekiyor. Ancak, kitlesel MIMO'nun baz istasyonundan gönderilecek sinyali üretmesi için ihtiyaç duyduğu yüksek sayıda anten ve elektronik devre elemanları pahalı olup, yüksek güç tüketebilir. Bu sorunu pratik olarak çözmek için daha ucuz ve daha az güç tüketen elektronik komponent kullanımı literatürde sıkça görülmektedir. Bunlardan özel olarak RF zincirindeki DAC'lara odaklanan çalışmalar vardır. Kitlesel MIMO dizisinde her antende düşük çözünürlüklü DAC'ların kullanılmasıyla, maliyet ve güç tüketimi azaltılabilir. Ancak, düşük çözünürlüklü DAC'ların kullanımı, nicemleme bozulmasını sistem performansını olumsuz etkileyebilen bir hale getirir. Bu bozulmayı azaltmak için, literatürde çeşitli nicemlemeli ön-kodlayıcı algoritmaları önerilmiştir. Bu çalışma, sembol oranından daha yüksek bir örnekleme hızına sahip olan aşırı örneklemeli DAC ile çalışan, yinelemeli ve bozulma bilincine sa-

hip ön-kodlayıcıyı sunar, çünkü üst örnekleme, kitlesel MIMO sistemlerinde nicemleme bozulmasını azaltmak için etkili bir yaklaşımdır. Önerdiğimiz ön-kodlayıcının, literatürdeki benzer hesaplama karmaşıklığına sahip mevcut aşırı örneklemeli ön-kodlayıcılardan daha iyi bir performans sergilediğini, iletim bandında hata oranı performansını etkin bir şekilde maksimize ederken dış bant emisyonları da minimize ettiğimizi gösteriyoruz. Ayrıca, önerilen ön-kodlayıcı ve nicemlemeli sıfıra zorlama (ZF) için, bitişik kanal bantlarında ve katlanma gibi çeşitli senaryolarda performans analizini gerçekleştiriyoruz.

Anahtar Kelimeler: yinelemeli ön-kodlayıcı, nicemleme, 1-bit dijital-analog dönüştürücü (DAC), kitlesel MIMO, aşırı örnekleme, çoklu-bit, geniş bant, frekans seçici kanal, aşağı bağlantı, sıfıra-zorlama.

To my dear family and all the loved ones

ACKNOWLEDGMENTS

I want to express my gratitude to my advisor, Assistant Professor Gökhan Muzaffer Güvensen. I started to love our EE department with the "EE230 PROBABILITY AND RANDOM VARIABLES" course, which was instructed by Gökhan Güvensen. More than the course material itself, I enjoyed our conversations about the course and probability. The following year, I also took the "EE301 SIGNALS AND SYSTEMS I" course from him, which allowed for deep discussions about signals. I appreciate both Gökhan Güvensen's attitude and the topics of signal and probability, which I have built my career around. Our relationship has grown stronger, and now we conduct research together in the area of wireless communication. His support, interest in communications, confidence, rigorous attitude, the friendship and mentorship he offered were priceless. I couldn't have succeeded without his help and inspiration. I am very grateful to him. One more time, thank you very much.

I am also grateful to Dr. Ali Bulut Üçüncü, with whom I had the privilege to conduct research. I have admired him since he was the assistant for the Communications course I took. His intellect, diverse way of looking at things, and calm attitude undoubtedly boosted the research quality of this study. I want to extend my gratitude to Prof. Ali Özgür Yılmaz for his ideas and valuable insights about communication theory. When I think of him, three things come to mind: strength, independence, and confidence, which I was able to see in myself more thanks to him.

I should also thank Vodafone Turkey for funding my graduate studies as part of the 5G and Beyond Joint Graduate Support Program, and the Information and Communication Technologies Authority of Turkey (BTK) for organizing this meaningful program to support research on communication technologies in our country.

My family plays the most important role in supporting me in every aspect of my life. Their love and happiness are the fundamental supports of my life. My mother, Belgin, and my father, Ömer, have always believed in my success in life, and this thesis may

be seen as a projection of that success into the academic part of my life. I am also thankful to my aunt, Seril, for her help during this period. Lastly, I thank all my loved ones for bringing joy to my life.

TABLE OF CONTENTS

LIST OF TABLES

TABLES

LIST OF FIGURES

FIGURES

LIST OF ABBREVIATIONS

AGC	Automatic Gain Controller
BER	Bit Error Rate
BS	Base Station
CSCG	Circularly Symmetric Complex Gaussian
CSI	Channel State Information
DAC	Digital-to-Analog Converter
DFT	Discrete Fourier Transform
EVM	Error-Vector Magnitude
IDAP	Iterative Distortion Aware Precoder
IDFT	Inverse Discrete Fourier Transform
LOS	Line of Sight
MIMO	Multiple Input Multiple Output
MU	Multi-User
OFDM	Orthogonal Frequency Division Multiplexing
OOB	Out-of-Band
PDP	Power Spectral Density
QAM	Quadrature Amplitude Modulation
QPSK	Quadrature Phase Shift Keying
RF	Radio-Frequency
Rx	Receiver
SER	Symbol Error Rate
SINR	Signal to Interference plus Noise Ratio
SNR	Signal to Noise Ratio
ULA	Uniform Linear Array

ZF	Zero-Forcing

CHAPTER 1

INTRODUCTION

Massive multiple-input multiple-output (MIMO) systems have attracted significant attention due to the remarkable advantages they provide regarding spectral and energy efficiency [1, 2]. Despite the advantages that massive MIMO systems offer, there are a number of practical implementation difficulties due to the very large number of antennas in such systems. One difficulty is related to the very high power consumption and cost associated with the data converters used in the RF chain of the massive MIMO system [3, 4]. To overcome this bottleneck, utilization of low-resolution digital-to-analog converters (DAC) with low power consumption and cost in massive MIMO systems has been examined in various studies [5, 6, 7, 8, 9, 2, 10, 11, 12, 13, 14, 3, 15, 16, 17]. While low-resolution DACs have low power consumption and cost, they introduce a significant distortion in the transmitted signal due to higher quantization noise. Although the distortion caused by quantization noise can be reduced by increasing the number of antennas, the linear precoders, such as zero-forcing (ZF) precoder, that are performing quite well for unquantized massive MIMO, can exhibit very inferior results with a high error-floor performance [18, Fig.3] for quantized case. Therefore, various alternative precoders are proposed for quantized massive MIMO showing improved performance under quantization [5, 6, 7, 8, 9, 2, 10, 11, 12, 16, 17, 13, 14, 3, 15]. In spite of the advantages provided by the proposed quantized precoders in terms of error-rate or achievable rate performance, some of them do not employ the technique of temporal oversampling, which is an effective way to mitigate quantization noise [3]. By increasing the temporal oversampling rate to a rate higher than the symbol rate, we benefit from spreading the quantization distortion to a larger bandwidth. This effectively reduces the distortion in the transmission bandwidth where the intented signal

lies. Thus, not using the temporal oversampling limits the performance of the non-oversampling quantized precoders proposed in various studies, some of which appear in [5, 6, 7, 8, 9, 2]. Therefore, quantized precoders that can work with oversampling DACs [10, 11, 12, 16, 17, 13, 14, 3, 15] in massive MIMO systems have appeared in a number of studies, achieving superior performance compared to the quantized non-oversampling MIMO precoders. In this work, we propose an iterative quantized precoder that is able to perform close to unquantized ideal precoders even under heavy quantization and outperform the existing quantized oversampling precoders of comparable complexity in the literature with respect to error-rate performance, while being able to minimize out-of-band (OOB) emissions. In the following section, we summarize the existing studies and discuss their weaknesses against the quantized precoding algorithm we propose.

1.1 Related Works

To begin with, [10] proposes a precoding scheme that employs oversampling to enable error-free detection of data symbols in the absence of noise and interference. However, a very important drawback of [10] is that the required transmission bandwidth is linearly increasing with the oversampling factor, e.g. 2 times oversampling expands the transmission bandwidth 2 times, while the transmission bandwidth of the precoder we propose does not change with the oversampling factor. On the contrary, OOB emissions decrease with increased oversampling factors for the proposed precoder in this work. Moreover, the precoder presented in [10] is limited to flat-fading channels, whereas the precoder we propose can work in frequency-selective channels. Similar bandwidth expansion and flat-fading channel requirements also exist in the studies [11, 12], which again employ temporal oversampling to enhance error-rate performance. Temporal oversampling is also used in [13] to improve the performance of the proposed MIMO precoder. However, the precoder in [13] is shown to work only in flat-fading channels and requires a special type of data converter, namely sigma-delta DACs, to be able to perform oversampling, whereas the DACs utilized in our work are usual 1-bit DACs that are only able to quantize the in-phase and quadrature parts of the signals to be transmitted. A recent study [15] also proposes a nonlinear

quantized precoder with temporal oversampling capability. However, the precoder in [15] requires solving a high dimensional optimization problem for each iteration of the precoder, which results in a much higher complexity compared to the proposed precoder in this work, as will be discussed in Chapter 3.4. In a more recent study, the authors of [19] propose a linear one-bit quantized oversampling precoder that achieves superior performance in terms of error-rate compared to the existing works under flat fading channel conditions. However, only a single step in a single iteration [19, Eqn. 40] of the optimization problem to find the precoder matrix by finding the dominant eigenvector of the covariance matrix associated with each user grows with the cube of the number of antennas [20, 21]. As the number of antennas is typically very large in massive MIMO systems, and the precoding matrix is found for every channel realization in fast-time in [19], the complexity of constructing the precoder matrix can be tremendous. The study [22] extends the precoder in [19] to multi-bit quantizers and frequency selective channels, although the similar computationally exhaustive steps also exist for the construction of the quantized precoder in [22]. Another study [14] proposes a nonlinear precoder that can work with oversampling DACs, thereby obtaining significantly improved error-rate performance. We discuss that the precoder in [14] has a comparable complexity to the proposed precoder in this work. The same study [14] and its version for flat-fading channels [5] is also selected as the main benchmark scheme in the recent studies [19] and [22], as [14] is stated to exhibit better performance than the linear quantized precoders [23, 24, 25, 26, 27], and comparable performance to the non-linear quantized precoders in [28, 29, 30]. Therefore, due to its comparable complexity to proposed precoder in our work and its superior and competent performance compared to existing quantized precoders, we consider the precoder SQUID [14] as the main benchmark precoder. We also benchmark the proposed precoder in this study with the oversampling ZF precoder in [3, 16, 17], as a comparable complexity oversampling precoder. According to the results we obtain, the proposed precoding algorithm significantly outperforms the benchmark precoders in terms of error-rate and/or OOB emission performance. We also show that the proposed precoder can achieve ideal unquantized ZF precoder performance in many cases.

Although there are numerous studies targeting improved error-rate or achievable rate

performance for quantized MIMO precoding, the studies that also try to minimize out-of-band emissions (OOB) while optimizing error-rate performance are relatively limited. However, especially for very low-resolution quantizers, non-linearity can result in very high OOB levels [3]. To cope with the resulting high OOB levels, employing an analog filter after DAC is one possible solution. Nonetheless, utilization of an analog filter does not come without any drawbacks. To begin with, it breaks off the orthogonality between the OFDM subcarriers. This can result in a significant error-rate performance degradation. For example, up to about 5 dB SNR loss can be observed due to analog filter utilization for one-bit quantized MIMO, as shown in [31]. Additional BER degradation will also be observed due to insertion losses and the noise figure introduced by the analog filter after DAC. Besides, if the filter is selected as a small order filter, the stopband attennuation can be less than 10 dB [32]. Higher order filters can be employed for higher stop-band attennuation, but due to the increased filter delay, the cyclic prefix length of the OFDM symbol should be increased. This results in an increased overhead, thereby reducing the spectral efficiency of the communication system. Therefore, there exists a number of studies that try to limit the OOB emissions when low-resolution quantizers are utilized before any analog filtering in a massive MIMO system [32, 31]. In [32], it is claimed that OOB emissions can be lowered by 10 dB in a one-bit quantized massive MIMO system, while the sum-rate is also maximized. However, the proposed technique requires non-convex optimization of $N_t N_s$ variables, where N_t is the number of antennas and N_s is the OFDM symbol length. This means that the precoder in [32] is highly infeasible in terms of computational complexity for massive MIMO systems, considering that N_t and N_s can be as large as 256 and 1024, respectively [2]. Therefore, we exclude this precoder in our benchmark schemes to achieve fair comparison grounds. In [31], a digital pre-distorter is used to suppress OOB in low-resolution quantized MIMO systems. The employed precoder is a linear ZF precoder, which we will demonstrate to provide very inferior performance compared to the proposed precoder in this study. The related works are also summarized as in Table 1.1.

Table 1.1: Summary of related works

Reference	**Weaknesses Compared to IDAP/Comments**
[10], [11], [12]	Bandwidth expansion, flat-fading requirement
[13]	Flat-fading and sigma-delta DAC requirement
[15], [19], [22], [32]	High computational complexity
[23]-[27]	Inferior performance than the benchmark [14]
[28]-[30]	Comparable performance to the benchmark [14]
[3], [14], [16], [17], [31]	Selected as benchmark precoders

1.2 Contributions

The contribution items related to this work can be summarized as follows:

- We propose an iterative precoder for quantized downlink wideband massive MIMO, named iterative distortion aware precoder (IDAP). We show that IDAP is able to outperform the existing state-of-the-art quantized oversampling massive MIMO precoders of comparable complexity.
- IDAP can minimize the distortion in the desired band, thus maximize error-rate performance, and jointly minimize the OOB emissions. If a certain portion of OOB is known to interfere with another band, it is shown that IDAP can achieve very low OOB levels for that portion of OOB, while maintaining competent error-rate performance in the desired band (in-band).
- We make the performance analysis of downlink quantized MIMO for oversampled precoders for both one and multi-bit quantizers. The proposed analysis is able to take into account the effect of an interfering base station in an adjacent band and provide accurate results. To the best of our knowledge, there is no study that makes the performance analysis for quantized downlink MIMO with oversampling under the effect of an interfering base station.
- The provided performance analysis is also able to take into account the effect of aliasing and anti-aliasing filters, thus able to reflect the impact of interfering base stations from frequency bands that are outside the sampling rate of the

precoder and the receiver (outside the frequency region between $-F_s/2$ and $F_s/2$, F_s being the sampling rate). To the best of our knowledge, there is no study that considers the effect of aliasing in the performance analysis of massive MIMO systems, although such analysis can be important as near-far effects can result in high interference from adjacent frequency bands, which anti-aliasing filters may not be able to tolerate.

- Our proposed analysis for linear quantized downlink MIMO precoder with oversampling retains validity even without interference from adjacent bands. This analysis is notably simpler than existing work [3], which involves large matrix (as large as $N_tU \times N_tU$, where N_t and U are the number of transmit antennas and users, respectively) inversions for precise results when overload distortion is not negligible relative to granular distortion. Our approach offers reduced complexity, only an inversion of $U \times U$ matrix. Moreover, even if some approximations for small overload distortion are provided in [3], in order not to take the inverse of such large matrices, the memory resources to hold such matrices can be very high for large N_t, which is typical in massive MIMO systems.

- We show that IDAP outperforms the benchmark precoders for many different scenarios involving an interfering base station from an adjacent band whose signal leaks to the in-band region due to aliasing.

1.3 Notation

a is scalar, $\mathbf{a}$ is column vector, $\mathbf{A}$ is matrix, $\mathbf{A}^*$, $\mathbf{A}^T$ and $\mathbf{A}^H$ represent the conjugate, transpose and Hermitian of matrix $\mathbf{A}$, respectively. $\mathbf{a}$ is in frequency domain and $\tilde{\mathbf{a}}$ is in time domain. $E[.]$ is expectation operator, $\Re(.)$ and $\Im(.)$ are real and imaginary operators with $j = \sqrt{-1}$. $||.||$ is Euclidian norm. $\mathrm{diag}(\mathbf{A})$ is diagonal matrix whose diagonal entries are same as $\mathbf{A}$. $\mathbf{0}_N$ is 0 vector with size $N \times 1$, $\mathbf{0}_{N\times M}$ is a zero matrix with size $N \times M$ and $\mathbf{I}_N$ is identity matrix with size $N \times N$. $[\mathbf{a}]_{(m)}$ means m^{th} entry of vector $\mathbf{a}$, and $[\mathbf{A}]_{(m,n)}$ means m^{th} row n^{th} column entry of matrix $\mathbf{A}$. $\mathbb{R}^{M\times N}$ and $\mathbb{C}^{M\times N}$ represents the set of real and complex vectors with size $M \times N$, respectively. Φ is the standard normal cumulative distribution function (CDF), which

is $\Phi(a) = \frac{1}{\sqrt{2\pi}} \int_{-\infty}^{a} e^{\frac{-x^2}{2}} dx$. $\mathcal{F}$ and $\mathcal{F}^{-1}$ takes the Discrete Fourier Transform (DFT) or inverse DFT (IDFT).

1.4 The Outline of the Thesis

The remainder of the thesis is organized as follows:

- Chapter 2 describes the system model used for downlink communication for MU-MIMO setup where OFDM is employed. It describes the transmitter and the receiver as well as the quantization model, and the channel model.
- In Chapter 3, the derivation of the proposed precoder, known as IDAP, is presented in the frequency domain. This derivation takes into account the effects of quantization and the interfering BS.
- Chapter 3.4 focuses on the computational complexity analysis of the IDAP precoder and compares it with other precoders to assess its efficiency.
- Chapter 4 contains the derivation of the SINR expressions of IDAP and quantized ZF to analyze their performance.
- Chapter 5 demonstrates the performance of the IDAP by comparing it with other benchmark precoders using Monte Carlo simulations to look at error-rate and OOB emissions.
- Chapter 6 concludes the thesis by providing a concise summary of the key findings and their implications.

CHAPTER 2

SYSTEM MODEL

This chapter delves into the discussion of the transmitter and receiver models for the downlink wireless communication system. The focus is on a scenario involving two base stations (BS) that cater to their respective users, but face potential interference due to factors such as proximity to the cell edge or the near-far effect. To facilitate the derivation, we initially consider a scenario where a single BS serves its users, and subsequently introduce the second BS to the analysis. The study considers an urban environment where multipath fading occurs, with the presence or absence of a line-of-sight (LOS) component. When there is no LOS component, the channel is modeled as experiencing Rayleigh fading, whereas when a LOS component is present, the channel is modeled as undergoing Rician fading. Notably, the transmitter employs a finite-bit DAC, leading to quantization of its signal, while the receiver does not employ quantization. Receiver decodes the received signal at receiver sampling rate by employing nearest neighborhood detection after scaling the constellation to unit power. Receiver doesn't employ any advanced decoding techniques.

2.1 Multi-Carrier Downlink Transmission

This study considers downlink OFDM transmission for a wideband massive MIMO system[1]. In this system, U single-antenna users communicate with a base station,

[1] Massive MIMO is choosed because number of transmit antennas must be notably larger than receiver antennas. The need for that is due to the quantization of the transmit signal from each antenna element. OFDM signal in time-domain looks like Gaussian signal realization due to Central-Limit-Theorem, which indicates that it contains many different amplitude levels in time domain; therefore, quantization heavily distorts it. Unless a large number of quantized signals are combined at the receiver side, there is no way to recover the OFDM signal. By addition of many quantized signals that passes from different channels, we are able to recover the OFDM signal, and detect the transmitted bits based on that.

equipped with N_t RF chains and antennas. For OFDM with K active subcarriers, oversampled message signal generated in frequency domain, namely $\mathbf{a}_k \in \mathbb{C}^{U\times 1}$, can be written as

$$\mathbf{a}_k = \begin{cases} \left[a_k^1\ a_k^2\ \dots\ a_k^U\right]^T & \text{if } k \in \mathcal{S}_a, \\ \mathbf{0}_U & \text{if } k \in \mathcal{S}_o, \end{cases} \tag{2.1}$$

where k is the frequency index, $\mathcal{S}_a = \{0, 1, ..., K/2-1, \mu K - K/2, \mu K - K/2 + 1, ..., \mu K - 1\}$ is the set of active (occupied) subcarriers, $\mathcal{S}_o = \{0, ..., \mu K - 1\} \backslash \mathcal{S}_a$ is the set of inactive subcarriers, and μ is the oversampling factor ($F_s = \mu K \Delta_s$, where Δ_s is subcarrier-spacing). For the occupied subcarriers, $E\left[|a_k^u|^2\right] = 1,\ \forall u$. Modulation symbols $\mathbf{a}_k$ (e.g. QAM), pass through precoding function $\boldsymbol{\phi}(.)$ to obtain $\mathbf{x}_k \in \mathbb{C}^{N_t\times 1}$ as follows:

$$\mathbf{x}_k = \left[x_k^1\ x_k^2\ \dots\ x_k^{N_t}\right]^T = \boldsymbol{\phi}(\mathbf{a}_k),\ k = 0, \dots, \mu K - 1. \tag{2.2}$$

The signal $\mathbf{x}_k$ is converted to time domain with IDFT $\mathcal{F}^{-1}$ to form $\tilde{\mathbf{x}}_n$ whose u^{th} entry can be found as

$$\tilde{x}_n^u = \mathcal{F}^{-1}\{x_k^u\} = \frac{1}{\sqrt{\mu K}} \sum_{k=0}^{\mu K-1} x_k^u e^{\frac{j2\pi kn}{\mu K}},\ \forall n, \tag{2.3}$$

where n is the time index. Then, $\tilde{\mathbf{x}}_n$ is fed to DACs to form quantized signal $\tilde{\mathbf{y}}_n$. The frequency domain counter-part of $\tilde{\mathbf{y}}_n$, namely $\mathbf{y}_k \in \mathbb{C}^{N_t\times 1}$, can be represented as

$$\mathbf{y}_k = \left[y_k^1\ y_k^2\ \dots\ y_k^{N_t}\right]^T = \mathcal{F}\left\{\boldsymbol{\psi}\left(\mathcal{F}^{-1}\{\mathbf{x}_k\}\right)\right\}, \tag{2.4}$$

where $\boldsymbol{\psi}(.)$ represents the nonlinear DAC operation.

2.2 Frequency-Selective Quantized Massive MIMO Channel Model

This section aims to present our quantization model for a finite bit DAC, followed by a comprehensive discussion of the channel model.

2.2.1 Nonlinearity Model for Finite Resolution DAC

We are utilizing a uniform mid-rise quantizer in our study, where the quantizer operates separately on the real and imaginary components of the input signal. The set of possible quantizer's output values is $\Theta = \{\ell_0, \ell_1, ..., \ell_{L-1}\}$ where $L = 2^q$ represents the number of possible real output values of the quantizer, and q is the number of DAC bits. The quantization thresholds are represented by the set $B = \{b_0, b_1, ..., b_L\}$, where $-\infty = b_0 < b_1 < ... < b_L = \infty$. We denote quantizer function as $\mathbf{Q}(.)$, which maps from the function space $\mathbb{R}^{N_t \times 1} \rightarrow \Theta^{N_t \times 1}$. The m^{th} element of the quantizer output, for an input $\mathbf{x} \in \mathbb{R}^{N_t \times 1}$, denoted as $[\mathbf{Q}(\mathbf{x})]_{(m)}$, is expressed as

$$[\mathbf{Q}(\mathbf{x})]_{(m)} = \ell_i, \text{ if } b_i < [\mathbf{x}]_{(m)} < b_{i+1}, \tag{2.5}$$

where $i \in \{0, 1, ..., L-1\}$. Using this notation, we describe the operation of the DAC function $\psi(.)$ for a complex input $\mathbf{x} \in \mathbb{C}^{N_t \times 1}$ as $\psi(\mathbf{x}) = \mathbf{Q}(\Re(\mathbf{x})) + j\mathbf{Q}(\Im(\mathbf{x}))$. Furthermore, for the uniform mid-rise quantizer, the output values are chosen as $\ell_i = \Delta(i - \frac{L}{2} + \frac{1}{2}), \quad i = 0, 1, ..., L-1$, and the threshold values are $b_i = \Delta(i - \frac{L}{2}), \quad i = 1, 2, ..., L-1$, Δ being the quantizer step size. Moreover, $\mathbf{x}_k$ is scaled by c_x such that $\frac{1}{\mu K}\sum_{k=0}^{\mu K-1} ||\mathbf{x}_k||^2 = N_t$ to ensure unit variance DAC input. This scaling is necessary since Δ will be adjusted assuming a unit-variance DAC input. To ensure that clipping is negligable, which will be important for the validity of the Bussgang gain matrix calculations which will be discussed in the following chapter, we adjust Δ as follows:

$$\Delta = \frac{2A_{clip}}{L}, \tag{2.6}$$

where the clipping amplitude A_{clip} is defined as $A_{clip} = \sqrt{1/2}\,(1 - \Phi^{-1}(P_c/2))$, with P_c being the desired clipping probability, and Φ^{-1} representing the inverse CDF of the standard normal distribution [2]. Subsequently, the DAC outputs are multiplied by c_y to ensure that $\mathbf{y}_k$ satisfies the desired average output power constraint of $\frac{1}{\mu K}\sum_{k=0}^{\mu K-1} ||\mathbf{y}_k||^2 = N_t$. Therefore, with input and output power scaling, (2.4) can be rewritten as

$$\mathbf{y}_k = c_y \mathcal{F}\left\{\boldsymbol{\psi}\left(\mathcal{F}^{-1}\{\mathbf{x}_k\}\right)\right\}, k = 0, \ldots, \mu K - 1. \tag{2.7}$$

[2] It is assumed that the DAC input follows a Gaussian distribution, which is a reasonable assumption for a time-domain OFDM signal due to the Central Limit Theorem.

2.2.2 Downlink MIMO Channel Model

Discarding the cyclic prefix, the received signal model in the frequency domain can be expressed as

$$\mathbf{r}_k = \begin{bmatrix} r_k^1 \; r_k^2 \; \ldots \; r_k^U \end{bmatrix}^T .k = 0, \ldots, \mu_c K - 1. \tag{2.8}$$

This notation allows us to represent $\mathbf{r}_k$ as

$$\mathbf{r}_k = \mathcal{F} \left\{ \sum_{p=0}^{P} \sigma_{(p)} \breve{\mathbf{H}}_p^H \breve{\breve{\mathbf{y}}}_{(\mathbf{n}-\mathbf{p})} \right\} + \boldsymbol{\nu}_k = \breve{\boldsymbol{\Omega}}_k^H \breve{\mathbf{y}}_k + \boldsymbol{\nu}_k \; , k = 0, \ldots, \mu_c K - 1, \tag{2.9}$$

where P represents the channel length, $\breve{\mathbf{H}}_p^H \in \mathbb{C}^{U \times N_t}$ is the time-domain downlink channel matrix associated with the p^{th} tap of the multipath channel, and $\sigma(p)^2$ denotes the channel power-delay profile (PDP). Here, $\frac{\mu_c}{\mu} F_s$ is a sampling rate, that can be much higher than the receiver sampling rate F_s, which will be important for incorporation of aliasing effects from subsequent channel bands [3]. In Equation (2.9), $\breve{\mathbf{y}}_k$ is the upsampled version of the $\mathbf{y}_k$ by a factor of μ_c/μ, obtained by padding the necessary amount of zeros as follows:

$$\begin{aligned} \breve{\mathbf{y}}_k &= \mathrm{up}(\mathbf{y}_k, \mu_c/\mu) \\ &\triangleq \begin{bmatrix} \mathbf{y}_0 \; \mathbf{y}_1 \; \cdots \; \mathbf{y}_{\mu K/2-1} \quad \mathbf{0}_{Nt \times \mu_c K - \mu K} \quad \mathbf{y}_{\mu K - \mu K/2} \; \mathbf{y}_{\mu K - \mu K/2 + 1} \; \cdots \; \mathbf{y}_{\mu K - 1} \end{bmatrix}, \end{aligned} \tag{2.10}$$

where $\mathrm{up}(., k)$ is the usual upsampling operation as defined in (2.10). Channel matrix $\breve{\boldsymbol{\Omega}}_k^H$ is constructed for $k = 0, ..., \mu_c K - 1$ from its time-domain counterpart $\breve{\mathbf{H}}_n^H$ by taking its $\mu_c K$ point DFT. The channel matrix $\breve{\mathbf{H}}_n$ can be written as

$$\breve{\mathbf{H}}_n = \begin{bmatrix} \mathbf{h}_n^1 \; \mathbf{h}_n^2 \; \ldots \; \mathbf{h}_n^U \end{bmatrix}, \; n = 0, \ldots, \mu_c K - 1. \tag{2.11}$$

The columns of channel matrix, namely $\mathbf{h}_n^u$, can be modeled with a circularly symmetric complex Gaussian (CSCG) distribution with mean $\mathbf{m}_{h_n^u} = E[\mathbf{h}_n^u]$, and covariance $\mathbf{C}_{\mathbf{h}_n^u} = E[\mathbf{h}_n^u (\mathbf{h}_n^u)^H]$ for the n^{th} channel tap associated with u^{th} user, which can be determined as [2], [33]

$$\mathbf{C}_{\mathbf{h}_n^u} = \int_{-\pi}^{\pi} \varrho_n^u(\theta) \mathbf{v}(\theta) \mathbf{v}^H(\theta) \, d\theta. \tag{2.12}$$

[3] It is worth noting that the introduction of μ_c may seem irrelevant at this point, but its importance will be clear when we introduce a 2^{nd} base station (BS) in the subsequent parts

Here, $\varrho_n^u(\theta)$ represents the angular power-delay profile of the n^{th} channel tap of user u, and $\mathbf{v}(\theta)$ is the steering vector of the antenna array. Without loss of generality, for a uniform linear array (ULA) with half-wavelength antenna separation, $\mathbf{v}(\theta) = \left[1; e^{j\theta}; ...; e^{j(Nt-1)\theta}\right]^T$, where $\theta = \pi \sin(\varphi)$, and φ being the angle of arrival. Assuming a uniform power distribution between $\theta_{u,1}^n$ and $\theta_{u,2}^n$, $\mathbf{C}_{\mathbf{h}_n^u}$ can be approximated for ULA and half-wavelength antenna separation as [2, 34]

$$\mathbf{C}_{\mathbf{h}_n^u} \approx \mathbf{v}(\kappa_{\theta,u}^n)\mathbf{v}(\kappa_{\theta,u}^n)^H \odot \mathbf{D}(\gamma_{\theta,u}^n), \tag{2.13}$$

where $\odot$ represents the Hadamard product, $\kappa_{\theta,u}^n = (\theta_{u,1}^n + \theta_{u,2}^n)/2$, $\gamma_{\theta,u}^n = |\theta_{u,1}^n - \theta_{u,2}^n|$, and $[\mathbf{D}(\theta)]_{(m,l)} = \text{sinc}((m-l)\theta/(2\pi))$, in which $\theta_{u,1}^n$ and $\theta_{u,2}^n$ is calculated using the mean arriving angle φ_u^n and angular spread ς_u^n as $\theta_{u,1}^n = \pi \sin(\varphi_u^n - \varsigma_u^n/2)$ and $\theta_{u,2}^n = \pi \sin(\varphi_u^n + \varsigma_u^n/2)$. Furthermore, the mean vector can be found as $\mathbf{m}_{h_n^u} = \sqrt{r_f}\mathbf{v}(\kappa_{\theta,u}^n)$ [33], where r_f represents the Rician factor which is calculated from the ratio of the line-of-sight (LoS) path power compared to the total power of non-LoS paths. In general, since the users and scatterers arising from distinct clusters, which correspond to different channel taps, are typically separated by multiple wavelengths in space, it is possible to consider the channels of different users and channel taps as statistically independent [33]. Here, the channel PDP satisfies $\sum_{p=0}^{P} \sigma_{(p)}^2 = 1/(1+r_f)$. The elements of the thermal noise $\boldsymbol{\nu}_k$ are i.i.d. zero-mean CSCG random variables with variance N_o.

CHAPTER 3

FREQUENCY-DEPENDENT NONLINEAR PRECODING: ITERATIVE DISTORTION AWARE PRECODER (IDAP)

In this chapter, we will derive the proposed precoder called IDAP. We will begin by defining an error $(\mathbf{\Omega}_k^H \mathbf{y}_k - \mathbf{a}_k)$ as the discrepancy between the error-free received signal $\mathbf{\Omega}_k^H \mathbf{y}_k$ and the message signal $\mathbf{a}_k$. Our objective is to minimize this error, aiming to achieve similarity between the received signal and the message signal. This similarity enables a basic nearest neighborhood decoder to determine the transmitted symbol. To achieve this goal, we employ Bussgang decomposition which can be used to linearize a nonlinear system in terms of its input and output while adding an uncorrelated noise term. Thus, the relationship between the precoded signal $\mathbf{x}_k$ and the output of the DAC $\mathbf{y}_k$ can be linearly defined. By utilizing Bussgang decomposition, we can obtain an iterative least-squares solution that considers the impact of quantization distortion. Through this process, we aim to effectively reduce the error. Then, we extend the precoder to effectively reduce the OOB emissions, where it hits the neighboring BS's users, called victim users. Finally, we present our algorithm and provide a block diagram illustrating the implementation of IDAP.

3.1 Bussgang Aided Problem Formulation

We want the noise free part of the received signal $\mathbf{r}_k$ to be as close to message signal $\mathbf{a}_k$ as possible, thus we will try to solve the following minimization problem by designing a proper precoder to calculate $\mathbf{x}_k$

$$\min_{\{\mathbf{x}_k\}} \sum_{k=0}^{\mu K-1} \left|\left|\mathbf{\Omega}_k^H \mathbf{y}_k - \mathbf{a}_k\right|\right|^2, \tag{3.1}$$

where the channel at the receiver sampling rate $\mathbf{\Omega}_k^H = \breve{\mathbf{\Omega}}_k^H$ for $k \in \{0, ..., \mu K/2 - 1\}$, and $\mathbf{\Omega}_k^H = \breve{\mathbf{\Omega}}_{k+(\mu_c-\mu)K}^H$ for $k \in \{\mu K/2, ..., \mu K - 1\}$. Also, $\{\mathbf{x}_k\}$ in the minimization indicates that minimization is done for whole sequence meaning $\mathbf{x}_k,\ \forall k$. The relation between $\mathbf{y}_k$ and $\mathbf{x}_k$ is described by (2.7), so our expression to minimize becomes

$$\min_{\{\mathbf{x}_k\}} \sum_{k=0}^{\mu K-1} \left|\left|\mathbf{\Omega}_k^H c_y \mathcal{F}\left\{\boldsymbol{\psi}\left(\mathcal{F}^{-1}\{\mathbf{x}_k\}\right)\right\} - \mathbf{a}_k\right|\right|^2. \tag{3.2}$$

It is hard to solve (3.2), owing to the nonlinear $\psi(.)$ and the fact that the size of $\mathbf{x}_k$ is large. Therefore, we resort to Bussgang Decomposition [35], decomposing a nonlinear system output into a linear function of the system input and a distortion term uncorrelated with input as

$$\mathbf{y}_k = \mathbf{A}\mathbf{x}_k + \boldsymbol{\eta}_k, \tag{3.3}$$

where $\mathbf{A} \in \mathbb{C}^{N_t \times N_t}$ denoted as Bussgang gain representing the linear part, whose specific selection makes the distortion $\boldsymbol{\eta}_k$ term uncorrelated with the DAC input. We will detail the selection of $\mathbf{A}$ subsequently, although we leave it as a general matrix at this stage. The equation in (3.3), is derived by assuming that DACs introduce a memoryless and time-invariant nonlinearity, and that the relationship between the DAC input $\tilde{\mathbf{x}}_n$ and output $\tilde{\mathbf{y}}_n$ in time-domain can be represented with a diagonal matrix $\mathbf{A}$, which is valid for a stationary scenario and scalar quantization. The Fourier transform preserves linearity, so the frequency-domain $\mathbf{A}$ is the same as its time-domain counterpart. By using Bussgang decomposition, the problem in (3.2) becomes

$$\min_{\{\mathbf{x}_k\}} \sum_{k=0}^{\mu K-1} \left|\left|\mathbf{\Omega}_k^H(\mathbf{A}\mathbf{x}_k + \boldsymbol{\eta}_k\{\mathbf{x}_k\}) - \mathbf{a}_k\right|\right|^2, \tag{3.4}$$

where $\boldsymbol{\eta}_k\{\mathbf{x}_k\}$ is written to show the dependency of instantaneous $\boldsymbol{\eta}_k$ to the sequence of $\{\mathbf{x}_k\}$, although they are statistically uncorrelated due to Bussgang decomposition. Moreover, this minimization can be decoupled for each frequency bin, since the summation in (3.4) is minimized when each term is minimized separately, so $\mathbf{x}_k$'s for different k's do not affect each other given $\boldsymbol{\eta}_k\{\mathbf{x}_k\}$[1]. Therefore, the minimization problem in (3.4) is equivalent to the following problem given $\boldsymbol{\eta}_k\{\mathbf{x}_k\}$ as

[1] We construct the minimization problem in the frequency domain to make variables uncorrelated, because if it would be constructed in time domain due to correlation the matrix size of the Bussgang gain matrix would be huge, which requires much more memory and computationally more costly to take inverse.

$$\min_{\{\mathbf{x}_k\}} \left|\left|\mathbf{\Omega}_k^H(\mathbf{A}\mathbf{x}_k + \boldsymbol{\eta}_k\{\mathbf{x}_k\}) - \mathbf{a}_k\right|\right|^2 \quad \forall k, \tag{3.5}$$

which tries to make the received signal $\mathbf{r}_k$ as close to $\mathbf{a}_k$ as possible in the occupied in-band subcarriers $\mathcal{S}_a$ where $\mathbf{a}_k$ is non-zero. Moreover, it also tries to make $\mathbf{r}_k$ close to $\mathbf{0}_U$ for the unoccupied OOB subcarriers $\mathcal{S}_o$, where $\mathbf{a}_k$ is zero. This facilitates reduced OOB emissions.

3.2 Nonlinear Frequency Domain Oversampled Precoding with Iterative Distortion Feedback

The difficulty with the problem in (3.5) is the fact that $\boldsymbol{\eta}_k\{\mathbf{x}_k\}$ depends on the sequence of $\mathbf{x}_k$, thus it is not a fixed entity. To address this issue, we observe that if $\boldsymbol{\eta}_k\{\mathbf{x}_k\}$ value was fixed and known, the solution for $\mathbf{x}_k$ in (3.5) could easily be found. That leads us to write an iterative solution as

$$\mathbf{x}_k^{(i)} = \underbrace{\mathbf{A}^{(i-1)^H}\mathbf{\Omega}_k(\mathbf{\Omega}_k^H\mathbf{A}^{(i-1)}\mathbf{A}^{(i-1)^H}\mathbf{\Omega}_k)^{-1}}_{\triangleq \mathbf{W}_k^{(i)}}\left[\mathbf{a}_k - \mathbf{\Omega}_k^H\boldsymbol{\eta}_k^{(i-1)}\right], \tag{3.6}$$

where the superscript (i) is the iteration index and $\boldsymbol{\eta}_k^{(i-1)}$ represents $\boldsymbol{\eta}_k\{\mathbf{x}_k^{(i-1)}\}$. Note also that $\mathbf{A}$ matrices in (3.6) are placed with a superscript as $\mathbf{A}^{(i)}$, meaning that the Bussgang gain matrices are also updated at each iteration. The reason for this update and how $\mathbf{A}^{(i)}$'s will be calculated will be explained in the subsequent parts. However, $\mathbf{x}_k^{(i)}$ in (3.6) may not satisfy the average power constraint $\frac{1}{\mu K}\sum_{k=0}^{\mu K-1}||\mathbf{x}_k^{(i)}||^2 = N_t$ for the DAC input vector. Therefore, we add a DAC input power scaling $c_x^{(i)}$ to (3.6) as follows:[2]

$$\mathbf{x}_k^{(i)} = c_x^{(i)}\mathbf{W}_k^{(i)}[\mathbf{a}_k - \frac{\mathbf{\Omega}_k^H\boldsymbol{\eta}_k^{(i-1)}}{c_x^{(i-1)}}]. \tag{3.7}$$

Here, for $k \in \mathcal{S}_a$, $\mathbf{x}_k^{(i)}$ aims to minimize the error-vector-magnitude (EVM) of the received data symbols by minimizing the discrepancy between the received signal $\mathbf{r}_k$ and the message signal $\mathbf{a}_k$. On the other hand, for $k \in \mathcal{S}_o$, $\mathbf{x}_k^{(i)}$ aims to mitigate the distortion signal $\boldsymbol{\eta}_k^{(i-1)}$ at the receiver side, leading to reduced OOB emissions. However, minimizing OOB emissions only at the position of our own user may not

[2] Division by $c_x^{(i-1)}$ for $\mathbf{\Omega}_k^H\boldsymbol{\eta}_k^{(i-1)}$ in (3.7) is necessary to cancel out distortion in the receiver side, which we will show in the subsequent parts.

be meaningful. Instead, our objective can be to suppress OOB emissions in areas where our signal may interfere with victim users served by a different base-station (BS), as illustrated in Fig. 3.1a. Different base-stations are denoted as BS_1 and BS_2 in Fig. 3.1a, each having N_t transmit antennas, serving user group UE^1 with U and user group UE^2 with U' users, respectively. The channels from BS_1 to UE^1, BS_1 to UE^2, BS_2 to UE^1 and BS_2 to UE^2 are denoted as $\mathbf{\Omega}_k^H$, $\overline{\mathbf{\Omega}}_k^H$, $\overline{\mathbf{\Lambda}}_k^H$ and $\mathbf{\Lambda}_k^H$, respectively. To cancel the distortion at the victim user side, we can modify (3.5) such that the interference channel between BS_1 and UE^2, namely $\overline{\mathbf{\Omega}}_k^H \in \mathbb{C}^{U' \times N_t}$, is taken into account. This modification aims to cancel the distortion in the victim users' side. Furthermore, it may not be necessary to cancel the distortion signal for all OOB subcarriers, reducing it in specific overlapping OOB subcarriers can be sufficient[3]. We denote these overlapping subcarriers as $\mathcal{S}_{ov}$. Accordingly, (3.7) can be reformulated as follows:

$$\mathbf{x}_k^{(i)} \triangleq \boldsymbol{\phi}(\mathbf{a}_k) = \begin{cases} c_x^{(i)} \mathbf{W}_k^{(i)} [\mathbf{a}_k - \frac{\mathbf{\Omega}_k^H \boldsymbol{\eta}_k^{(i-1)}}{c_x^{(i-1)}}] & \text{if } k \in \mathcal{S}_a, \\ -c_x^{(i)} \mathbf{W}_k^{(i)} \frac{\overline{\mathbf{\Omega}}_k^H \boldsymbol{\eta}_k^{(i-1)}}{c_x^{(i-1)}} & \text{if } k \in \mathcal{S}_{ov}, \\ \mathbf{0}_{Nt} & \text{if } k \in \mathcal{S}_o \backslash \mathcal{S}_{ov}, \end{cases} \tag{3.8}$$

where

$$\mathbf{W}_k^{(i)} = \begin{cases} \mathbf{A}^{(i-1)^H} \mathbf{\Omega}_k (\mathbf{\Omega}_k^H \mathbf{A}^{(i-1)} \mathbf{A}^{(i-1)^H} \mathbf{\Omega}_k)^{-1} & \text{if } k \in \mathcal{S}_a, \\ \mathbf{A}^{(i-1)^H} \overline{\mathbf{\Omega}}_k (\overline{\mathbf{\Omega}}_k^H \mathbf{A}^{(i-1)} \mathbf{A}^{(i-1)^H} \overline{\mathbf{\Omega}}_k)^{-1} & \text{if } k \in \mathcal{S}_{ov}. \end{cases} \tag{3.9}$$

In (3.9), at non-overlapping OOB subcarriers that is outside of $\mathcal{S}_{ov}$, we treated the channel in (3.5) as all zeros to ignore that OOB region which gives us the solution $\mathbf{x}_k = \mathbf{0}_{Nt}$. For the first iteration ($i = 1$), to find $\mathbf{x}_k^{(1)}$, we need to know $\boldsymbol{\eta}_k^{(0)}$, which can be initialized as $\boldsymbol{\eta}_k^{(0)} = \mathbf{0}_{N_t}$. For the following iterations, $\boldsymbol{\eta}_k^{(i)}$ is estimated by using (3.3) as

$$\boldsymbol{\eta}_k^{(i)} = \mathbf{y}_k^{(i)} - \mathbf{A}^{(i)} \mathbf{x}_k^{(i)} = c_y \mathcal{F} \left\{ \boldsymbol{\psi} \left(\mathcal{F}^{-1} \{ \mathbf{x}_k^{(i)} \} \right) \right\} - \mathbf{A}^{(i)} \mathbf{x}_k^{(i)}. \tag{3.10}$$

This process of calculating $\mathbf{x}_k^{(i)}$ then updating $\boldsymbol{\eta}_k^{(i)}$ continues until a desired number of iterations are performed. If the variables in the final iteration is denoted by the

[3] Here, notice that the precoder suppresses the OOB emissions only at the specific user locations e.g. it doesn't suppress OOB everywhere. Suppressing OOB everywhere means that we have removed all the quantization distortion (OOB is present due to only distortion). What this implies is that at the DAC output we should observe original OFDM signal e.g. without clipping. This is impossible, since we are employing a finite-bit DAC. Therefore, removing/suppressing OOB emission means removing it from specific locations, and distributing it on every other location.

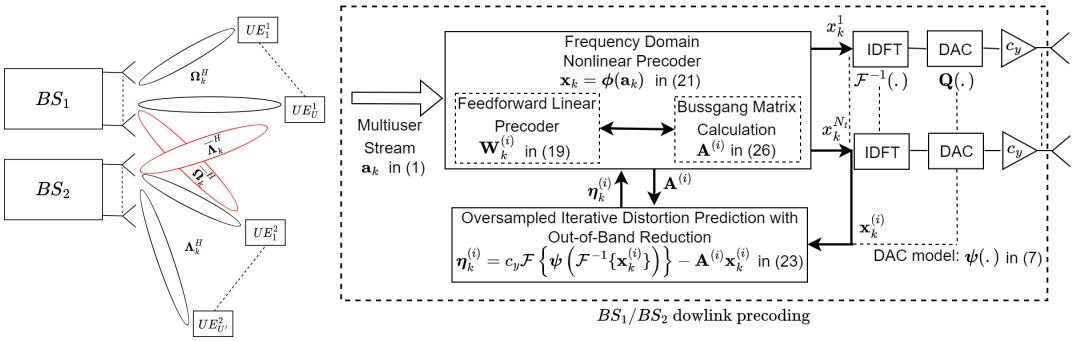

(a) 2 BS Downlink Scenario (b) IDAP Precoding Structure

Figure 3.1: Downlink Scenario with 2 BS and Precoding Structure

superscript $^{(*)}$, focusing on subcarriers $k \in \mathcal{S}_a$, and assuming $c_x^{(i)}$ converged to $c_x^{(*)}$ [4], the final output of the precoder $\mathbf{x}_k^{(*)}$ becomes

$$\mathbf{x}_k^{(*)} = \mathbf{A}^{(*)H}\mathbf{\Omega}_k \left(\mathbf{\Omega}_k^H \mathbf{A}^{(*)}\mathbf{A}^{(*)H}\mathbf{\Omega}_k\right)^{-1}\left[c_x^{(*)}\mathbf{a}_k - \mathbf{\Omega}_k^H \boldsymbol{\eta}_k^{(*)}\right]. \tag{3.11}$$

This $\mathbf{x}_k^{(*)}$ is fed to DAC that outputs $\mathbf{y}_k^{(*)} = \mathbf{A}^{(*)}\mathbf{x}_k^{(*)} + \boldsymbol{\eta}_k$. After passing through the channel, the noise-free received signal $\mathbf{r}_k \in \mathbb{C}^{U\times 1}$ can be represented as

$$\begin{aligned}
\mathbf{r}_k &= \mathbf{\Omega}_k^H \mathbf{y}_k^{(*)} = \mathbf{\Omega}_k^H\left[\mathbf{A}^{(*)}\mathbf{x}_k^{(*)} + \boldsymbol{\eta}_k\right] \\
&= \mathbf{\Omega}_k^H \mathbf{A}^{(*)}\mathbf{A}^{(*)H}\mathbf{\Omega}_k \left(\mathbf{\Omega}_k^H \mathbf{A}^{(*)}\mathbf{A}^{(*)H}\mathbf{\Omega}_k\right)^{-1}\left[c_x^{(*)}\mathbf{a}_k - \mathbf{\Omega}_k^H \boldsymbol{\eta}_k^{(*)}\right] + \mathbf{\Omega}_k^H \boldsymbol{\eta}_k \\
&= c_x^{(*)}\mathbf{a}_k + \mathbf{\Omega}_k^H\left[\boldsymbol{\eta}_k - \boldsymbol{\eta}_k^{(*)}\right] \approx c_x^{(*)}\mathbf{a}_k.
\end{aligned} \tag{3.12}$$

The approximation in the last line of (3.12) is accurate when the distortion estimate $\boldsymbol{\eta}_k^{(*)}$ converges to the true distortion term $\boldsymbol{\eta}_k$. In that case, the received signal is just a scalar multiple of the transmitted data symbols without any distortion. The scalar multiple can be canceled with a simple automatic gain control (AGC) operation at the receiver side. Also, for overlapping subcarriers $k \in \mathcal{S}_{ov}$, expression in (3.12) implies that received signal will be close to $\mathbf{0}_U$ since $\mathbf{a}_k$ is $\mathbf{0}_U$ for overlapping subcarriers, resulting in reduced OOB emissions.

[4] Empirically we observed that $c_x^{(i)}$ converges after a few iterations.

3.3 Bussgang Decomposition for Feedforward Precoding

Bussgang gain matrix $\mathbf{A^{(i)}}$ can be written as [5]

$$\mathbf{A}^{(i)} = \frac{c_y \Delta}{\sqrt{\pi}} \operatorname{diag}(\mathbf{C_x}^{(i)})^{-0.5} \sum_{n=1}^{2^q-1} \exp\left(-\Delta^2 \left(n - 2^{q-1}\right)^2 \operatorname{diag}(\mathbf{C_x}^{(i)})^{-1}\right), \quad (3.13)$$

where q is the number of bits as defined before, c_y is the DAC output scaling and $\mathbf{C_x}^{(i)}$ is the auto-covariance matrix of the DAC input signal at the i^{th} iteration of the precoder. Matrix $\mathbf{C_x}^{(i)}$ cannot easily be found analytically as $\mathbf{x}_k^{(i)}$ contains both $\mathbf{a}_k$ and $\boldsymbol{\eta}_k^{(i-1)}$, which are correlated[5]. To obtain a tractable analytical expression for $\mathbf{A}^{(i)}$, we assumed that received distortion power is negligible, which is an accurate assumption if the distortion power gets smaller with each iteration of the proposed distortion cancellation algorithm. This makes

$$\mathbf{C_x}^{(i)} \approx \left(\frac{\left(c_x^{(i)}\right)^2}{\mu K} \sum_{k \in \mathcal{S}_a} \mathbf{W}_k^{(i)} \mathbf{W}_k^{(i)H}\right), \quad (3.14)$$

which can be used in (3.13) to find $\mathbf{A}^{(i)}$. The algorithm flow of IDAP is summarized in Alg. 1. The block diagram of IDAP is shown on Fig. 3.1b.

3.4 COMPUTATIONAL COMPLEXITY AND BENCHMARK SELECTION

Regarding the computational complexity of IDAP, we focus on per-iteration complexity, as it constitutes the main item in the total computational complexity. Moreover, it will be seen in Chapter 5 that the necessary number of iterations for IDAP to converge is about 20 for many cases. The complexity per-iteration is mainly determined by the calculation of the precoder in line 11 and 15 of Algorithm 1, which result in a total complexity of $\mathcal{O}(U^2 N_t K') + \mathcal{O}(U^3 K')$, where $K' = K + |\mathcal{S}_{ov}|$. This is equal to the complexity of the linear ZF precoder per subcarrier. Therefore, we can

[5] Bussgang makes $\mathbf{x}_k$ and $\boldsymbol{\eta}_k$ uncorrelated. Since they are zero-mean, $E\left[\mathbf{x}_k \boldsymbol{\eta}_k^H\right] = \mathbf{0}_{N_t x N_t}$. Moreover, as $\mathbf{x}_k = \mathbf{B}_k \mathbf{a}_k - \mathbf{F}_k \boldsymbol{\eta}_k$, where $\mathbf{B}_k = c_x \mathbf{W}_k$, $\mathbf{F}_k = \mathbf{W}_k \boldsymbol{\Omega}_k^H$ (assuming c_x is converged) from (3.7), it follows that $E\left[\mathbf{x}_k \boldsymbol{\eta}_k^H\right] = E\left[\left(\mathbf{B}_k \mathbf{a}_k - \mathbf{F}_k \boldsymbol{\eta}_k\right) \boldsymbol{\eta}_k^H\right] = \mathbf{0}_{N_t x N_t}$ which makes $E\left[\mathbf{a}_k \boldsymbol{\eta}_k^H\right] \neq 0$ implying that $\mathbf{a}_k$ and $\boldsymbol{\eta}_k$ are correlated.

[6] c_A is used to control the convergence rate in the close-loop structure of IDAP. From empirical observations, it is observed that optimal c_A maximizing the error-rate performance of IDAP depends essentially only on q, and can be found offline.

Algorithm 1 IDAP

Initialization

$\boldsymbol{\eta}_k^{(0)} = \mathbf{0}_{N_t}$

$c_x^{(0)} = 1$

for $\forall k \in \mathcal{S}_a$ **do**

  $\mathbf{W}_k^{(0)} = \boldsymbol{\Omega}_k(\boldsymbol{\Omega}_k^H\boldsymbol{\Omega}_k)^{-1}$.

end for

set $\mathbf{A}^{(0)}$using (3.13) and (3.14) by taking $c_y = 1$

Iteration loop

for $i = 1\ to\ N_{it}$ **do**

  for $k \in \mathcal{S}_a$ **do**

    $\mathbf{W}_k^{(i)} = \mathbf{A}^{(i-1)^H}\boldsymbol{\Omega}_k\left(\boldsymbol{\Omega}_k^H\mathbf{A}^{(i-1)}\mathbf{A}^{(i-1)^H}\boldsymbol{\Omega}_k\right)^{-1}$

    $\mathbf{b}_k^{(i)} = \mathbf{W}_k^{(i)}\left[\mathbf{a}_k - \frac{\boldsymbol{\Omega}_k^H\boldsymbol{\eta}_k^{(i-1)}}{c_x^{(i-1)}}\right]$

  end for

  for $k \in \mathcal{S}_{ov}$ **do**

    $\mathbf{W}_k^{(i)} = \mathbf{A}^{(i-1)^H}\overline{\boldsymbol{\Omega}}_k(\overline{\boldsymbol{\Omega}}_k^H\mathbf{A}^{(i-1)}\mathbf{A}^{(i-1)^H}\overline{\boldsymbol{\Omega}}_k)^{-1}$

    $\mathbf{b}_k^{(i)} = -\mathbf{W}_k^{(i)}\frac{\overline{\boldsymbol{\Omega}}_k^H\boldsymbol{\eta}_k^{(i-1)}}{c_x^{(i-1)}}$

  end for

  for $k \in \mathcal{S}_o\backslash\mathcal{S}_{ov}$ **do**

    $\mathbf{b}_k^{(i)} = \mathbf{0}_{Nt}$

  end for

  $c_x^{(i)} = \sqrt{N_t\mu K/\sum_{k=0}^{\mu K-1}||\mathbf{b}_k^{(i)}||^2}$

  $\mathbf{x}_k^{(i)} = c_x^{(i)}\mathbf{b}_k^{(i)}$

  $\mathbf{y}_k^{(i)} = \mathcal{F}\left\{\boldsymbol{\psi}\left(\mathcal{F}^{-1}\{\mathbf{x}_k^{(i)}\}\right)\right\}$

  $c_y^{(i)} = \sqrt{N_t\mu K/\sum_{k=0}^{\mu K-1}||\mathbf{y}_k^{(i)}||^2}$

  $\mathbf{y}_k^{(i)} = c_y^{(i)}\mathbf{y}_k^{(i)}$

  update $\mathbf{A}^{(i)}$ by using (3.13) and (3.14), then $\mathbf{A}^{(i)} = c_A\mathbf{A}^{(i)}$ [6]

  $\boldsymbol{\eta}_k^{(i)} = \mathbf{y}_k^{(i)} - \mathbf{A}^{(i)}\mathbf{x}_k^{(i)}$

end for

state that the overall computational complexity of IDAP is comparable to that of the linear ZF precoder. Regarding the existing precoders that employ oversampling in the literature, the computational complexity per-iteration of the precoder in [15] for frequency-selective channels is $\mathcal{O}(U^3K^3)$, only for the gradient calculation in [15, Eqn. 43], in addition to $\mathcal{O}(N_t^2K^2)$ complexity to calculate a constant in [15, Eqn. 44]. Their summation $\mathcal{O}(U^3(K')^3) + \mathcal{O}(N_t^2(K')^2)$ is much larger compared to the linear ZF precoder complexity $\mathcal{O}(U^3(K')) + \mathcal{O}(U^2N_t(K'))$, as $N_tK' >> U^2$ for a typical massive MIMO-OFDM scenario. The complexity of another oversampling precoder proposed in [14] is also stated to be comparable to the complexity of the ZF precoder per each subcarrier. Therefore, we will benchmark our precoder against the precoder in [14], in addition to the linear ZF precoder.

CHAPTER 4

PERFORMANCE ANALYSIS FOR IDAP AND QUANTIZED ZF

In this chapter, our focus is on deriving the signal-to-interference-plus-noise ratio (SINR) expressions for IDAP and quantized ZF in the presence of an interfering BS at the adjacent band. The interference can occur either through direct leakage or aliasing. The SINR expression for IDAP will incorporate two covariance matrices: the distortion covariance matrix of the intended BS and the DAC output covariance matrix of the interfering BS. Due to the absence of closed-form analytical expression for IDAP, these two covariance matrices need to be determined experimentally using a Monte Carlo approach. On the other hand, for the quantized ZF precoder, we will provide a fully analytical expression for the SINR by utilizing known equations for covariance matrices that undergo quantization. Moreover, our analysis for quantized ZF can be easily applied to all linear precoders by just taking the precoding matrix as the desired linear precoding matrix. By deriving these SINR expressions, we will conduct a comprehensive performance analysis of both precoders, considering the presence of interference from adjacent bands and accounting for the effects of covariance matrices and quantization.

4.1 SINR expressions of IDAP and Quantized ZF

From this point on, we focus on the case of two neighboring base-stations operating in adjacent frequency bands. A user in the first cluster, namely UE^1, receives signal from both base-stations, one as a desired signal from its base-station BS_1 through the channel $\breve{\mathbf{\Omega}}_k^H$, other as interference from neighboring base-station BS_2 through the channel $\breve{\overline{\mathbf{\Lambda}}}_k^H$. Also, the channel between BS_1 and UE^2 is referred to as $\overline{\mathbf{\Omega}}_k^H$, and the

channel between BS_2 and UE^2 is represented by $\mathbf{\Lambda}_k^H$, as depicted in Fig. 3.1a. It is assumed that both BSs use the same precoding, IDAP or ZF. To be able to account for aliasing effects over a wider bandwidth (wider than the DAC bandwidth of F_s), we introduce a sampling rate $\frac{\mu_c}{\mu}F_s >> F_s$ at this point. The received signal sampled at the rate $\frac{\mu_c}{\mu}F_s$ can be written as

$$\mathbf{f}_k = \begin{bmatrix} f_k^1 & f_k^2 & \dots & f_k^U \end{bmatrix}^T, k = 0, \dots, \mu_c K - 1, \tag{4.1}$$

where f_k^u is the received signal by the u^{th} user at the k^{th} subcarrier. The corresponding frequency-domain channel is

$$\breve{\mathbf{\Omega}}_k^H = \begin{bmatrix} \boldsymbol{\lambda}_k^1 & \boldsymbol{\lambda}_k^2 & \dots & \boldsymbol{\lambda}_k^U \end{bmatrix}^H, k = 0, \dots, \mu_c K - 1, \tag{4.2}$$

$[\boldsymbol{\lambda}_k^u]^H \in \mathbb{C}^{1\times Nt}$. Therefore, the received signal f_k^u user when IDAP is employed becomes

$$\begin{aligned} f_k^u &= g_k \left[[\boldsymbol{\lambda}_k^u]^H \breve{\mathbf{y}}_k^{(i_f)} + [\overline{\boldsymbol{\lambda}}_k^u]^H \breve{\overline{\mathbf{y}}}_{(k-\Delta f)_{\mu_c K}} + \nu_k^u \right] \\ &= g_k \left[[\boldsymbol{\lambda}_k^u]^H [\mathbf{A}^{(i_f-1)} \breve{\mathbf{x}}_k^{(i_f)} + \breve{\boldsymbol{\eta}}_k^{(i_f-1)}] + [\overline{\boldsymbol{\lambda}}_k^u]^H \breve{\overline{\mathbf{y}}}_{(k-\Delta f)_{\mu_c K}} + \nu_k^u \right] \\ &= g_k \underbrace{c_x^{(i_f)} \breve{a}_k^u}_{\text{message}} + g_k \underbrace{[\boldsymbol{\lambda}_k^u]^H [\breve{\boldsymbol{\eta}}_k^{(i_f-1)} - \widehat{\boldsymbol{\eta}}_k^{(i_f-1)}]}_{\triangleq e_k^u, \text{ distortion}} + g_k \underbrace{[\overline{\boldsymbol{\lambda}}_k^u]^H \breve{\overline{\mathbf{y}}}_{(k-\Delta f)_{\mu_c K}}}_{\triangleq \xi_k^u, \text{ interference}} + \underbrace{g_k \nu_k^u}_{\text{noise}} \\ &= g_k c_x^{(i_f)} \breve{a}_k^u + g_k e_k^u + g_k \xi_k^u + g_k \nu_k^u, \end{aligned} \tag{4.3}$$

where i_f is the final iteration index, $\widehat{\boldsymbol{\eta}}_k^{(i_f-1)} = \breve{\mathbf{y}}_k^{(i_f-1)} - \mathbf{A}^{(i_f-1)} \breve{\mathbf{x}}_k^{(i_f-1)}$ is the estimated distortion obtained as in line 27 of the Algorithm 1, $\breve{\boldsymbol{\eta}}_k^{(i_f-1)} \triangleq \breve{\mathbf{y}}_k^{(i_f)} - \mathbf{A}^{(i_f-1)} \breve{\mathbf{x}}_k^{(i_f)}$. Moreover, $\breve{\mathbf{x}}_k^{(i)} = \text{up}(\mathbf{x}_k^{(i)}, \mu_c/\mu)$, which is upsampled version of $\mathbf{x}_k^{(i)}$ by μ_c/μ and $\breve{\mathbf{a}}_k = \text{up}(\mathbf{a}_k, \mu_c/\mu)$. Furthermore, $[\overline{\boldsymbol{\lambda}}_k^u]^H$ is the u^{th} row of BS_2's channel $\breve{\overline{\mathbf{\Lambda}}}_k^H$, and ν_k^u is zero-mean Gaussian white noise with variance N_o. In addition, $\breve{\overline{\mathbf{y}}}_{(k-\Delta f)_{\mu_c K}}$ is obtained from the transmitted signal of BS_2, namely $\breve{\overline{\mathbf{y}}}_k$, with a circular shift by Δf modulo $\mu_c K$. $\breve{\overline{\mathbf{y}}}_k$ is defined similar to $\breve{\mathbf{y}}_{(k)}$ as in (2.1)-(2.4) and (2.10) by replacing the transmit symbols of BS_1, namely $\mathbf{a}_k$, by the transmit symbols of BS_2. The IF filter gain is represented by g_k, which is assumed to be equal to 1 within the bandwidth of μK subcarriers where the transmitted signal is located (i.e., the first and last $\mu K/2$ subcarriers), and ϵ outside of this range. Δf is the frequency shift of the transmitted signal of BS_2 to align its transmission bandwidth. In Fig. 4.1, $\breve{\mathbf{y}}_k^{(i_f)}$, $\breve{\overline{\mathbf{y}}}_{(k-\Delta f)_{\mu_c K}}$, and g_k is visualized to gain insight for $K \leqslant \Delta f \leqslant \mu K/2$. As Δf increases in this range, there would be less direct overlap, but more aliasing if $\epsilon \neq 0$. Also, one inband

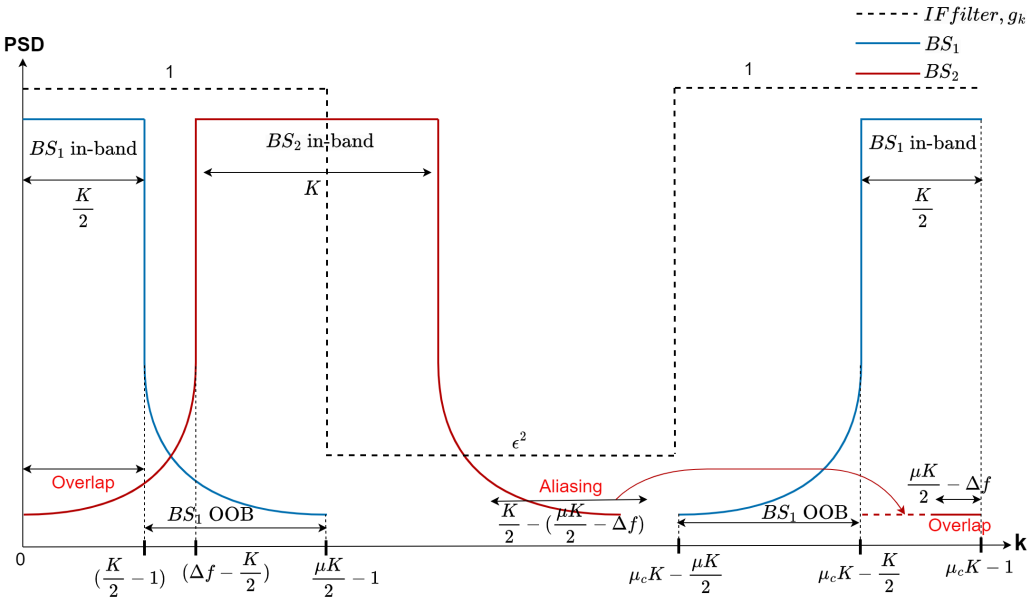

Figure 4.1: Power spectral density (PSD) vs frequency-index of transmitted signals from BS_1 and BS_2, IF filter g_k for adjacent channel interference case due to both OOB overlap and aliasing

subcarrier of BS_1 is interfered by at most one subcarrier of BS_2 depending on Δf and ϵ. Even if OOB suppression of the IF filter is high (for small ϵ), it may not be adequate due to near-far effects [36]. To obtain the transmitted signal for quantized ZF precoder, the frequency domain precoded signal can be written as

$$\mathbf{x}_k^{ZF} = c_x^{ZF} \underbrace{\mathbf{\Omega}_k (\mathbf{\Omega}_k^H \mathbf{\Omega}_k)^{-1}}_{\triangleq \mathbf{W}_k^{ZF}} \mathbf{a}_k, \tag{4.4}$$

where c_x^{ZF} is DAC input power scaling for ZF. Then, DAC output is obtained as follows:

$$\mathbf{y}_k^{ZF} = c_y^{ZF} \mathcal{F} \left\{ \boldsymbol{\psi} \left(\mathcal{F}^{-1} \{ \mathbf{x}_k^{ZF} \} \right) \right\}, k = 0, \ldots, \mu K - 1, \tag{4.5}$$

which can be expressed by using Bussgang decomposition as

$$\mathbf{y}_k^{ZF} = \mathbf{A}^{ZF} \mathbf{x}_k^{ZF} + \boldsymbol{\eta}_k^{ZF}, \tag{4.6}$$

where $\mathbf{x}_k^{ZF}$ and $\boldsymbol{\eta}_k^{ZF}$ are uncorrelated. Bussgang gain matrix $\mathbf{A}^{ZF}$ can be found with

$$\mathbf{A}^{ZF} = \frac{c_y^{ZF} \Delta}{\sqrt{\pi}} \operatorname{diag}(\mathbf{C}_x^{ZF})^{-0.5} \sum_{n=1}^{2^q - 1} \exp\left(-\Delta^2 \left(n - 2^{q-1} \right)^2 \operatorname{diag}(\mathbf{C}_x^{ZF})^{-1} \right), \tag{4.7}$$

where $\mathbf{C}_x^{ZF} = \frac{1}{\mu K}\sum_{k\in\mathcal{S}_a}(c_x^{ZF})^2\mathbf{W}_k^{ZF}(\mathbf{W}_k^{ZF})^H$. Then, received signal for the u^{th} user for ZF precoder becomes,

$$\begin{aligned} f_k^u &= g_k\left[[\boldsymbol{\lambda}_k^u]^H\breve{\mathbf{y}}_k^{ZF} + [\overline{\boldsymbol{\lambda}}_k^u]^H\breve{\overline{\mathbf{y}}}_{(k-\Delta f)_{\mu_c K}}^{ZF} + \nu_k^u\right] \\ &= g_k\left[[\boldsymbol{\lambda}_k^u]^H[\mathbf{A}^{ZF}\breve{\mathbf{x}}_k^{ZF} + \breve{\boldsymbol{\eta}}_k^{ZF}] + [\overline{\boldsymbol{\lambda}}_k^u]^H\breve{\overline{\mathbf{y}}}_{(k-\Delta f)_{\mu_c K}}^{ZF} + \nu_k^u\right] \\ &= g_k c_x^{ZF}\underbrace{[\boldsymbol{\lambda}_k^u]^H\mathbf{A}^{ZF}\mathbf{W}_k^{ZF}}_{\triangleq\mathbf{h}_k'^{ZF},\text{ effective channel}}\breve{\mathbf{a}}_k + g_k\underbrace{[\boldsymbol{\lambda}_k^u]^H\breve{\boldsymbol{\eta}}_k^{ZF}}_{\triangleq e_k,\text{ distortion}} + g_k\underbrace{[\overline{\boldsymbol{\lambda}}_k^u]^H\breve{\overline{\mathbf{y}}}_{(k-\Delta f)_{\mu_c K}}^{ZF}}_{\triangleq\xi_k,\text{ interference}} + \underbrace{g_k\nu_k^u}_{\text{noise}}, \end{aligned} \tag{4.8}$$

where $\breve{\mathbf{y}}_k^{ZF} = \mathrm{up}(\mathbf{y}_k^{ZF}, \mu_c/\mu)$, $\breve{\mathbf{x}}_k^{ZF} = \mathrm{up}(\mathbf{x}_k^{ZF}, \mu_c/\mu)$, $\breve{\boldsymbol{\eta}}_k^{ZF} = \mathrm{up}(\boldsymbol{\eta}_k^{ZF}, \mu_c/\mu)$, and $\breve{\overline{\mathbf{y}}}_k^{ZF}$ is defined similar to $\breve{\mathbf{y}}_k^{ZF}$ as in (4.4)-(4.5), by replacing the transmit symbols of BS_1, namely $\mathbf{a}_k$, by the transmit symbols of BS_2. Since $\boldsymbol{\Omega}_k^H\mathbf{A}^{ZF}\mathbf{W}_k^{ZF}$ is not diagonal, unlike IDAP where matrix $\mathbf{A}$ is predicted and cancelled, multi-user interference (MUI) exists in the received signal for the u^{th} user. Therefore, the received signal f_k^u for ZF precoder can be written as

$$f_k^u = g_k\alpha_k^u\breve{a}_k^u + g_k\underbrace{\sum_{l=1,l\neq u}^{U}\alpha_k^l\breve{a}_k^l}_{\triangleq m_k^u,\text{ MUI}} + g_k e_k^u + g_k\xi_k^u + g_k\nu_k^u, \tag{4.9}$$

where the intended user gain $\alpha_k^u = c_x^{ZF}\left[\mathbf{h}_k'^{ZF}\right]_u$, $\left[\mathbf{h}_k'^{ZF}\right]_u$ being the u^{th} element of the effective channel vector, and multi-user interference gain $\alpha_k^l = c_x^{ZF}\left[\mathbf{h}_k'^{ZF}\right]_l$. Here, we also define the signal sampled at the receiver sampling rate F_s, namely $\mathbf{r}_k \in \mathbb{C}^{U\times 1}$, as

$$\mathbf{r}_k = \left[r_k^1\ r_k^2\ \ldots\ r_k^U\right]^T, k = 0,\ldots,\mu K-1. \tag{4.10}$$

According to the following proposition, the received signal by the uth user, namely r_k^u, can be found in terms of f_k^u, which will enable us to take into account the effect of aliasing on the receiver side signal-to-interference-plus-noise ratio (SINR).

Proposition 1. *r_k^u can be found from f_k^u as*

$$r_k^u = \frac{\mu}{\mu_c}\sum_{m=0}^{\frac{\mu_c}{\mu}-1} f_{(k-m\mu K)_{\mu_c K}}^u, \tag{4.11}$$

where downsampling rate is μ_c/μ. [1]

[1] Downsampling f_k^u to rate μ implies there will be aliasing to terms contained in the f_k^u that has bandwidth larger than μK. Terms with bandwidth up to μK wouldn't suffer from aliasing.

Proof. See Appendix A.1. □

Using (4.3), (4.9) and (4.11), we obtain the following result:

$$\begin{aligned} r_k^u &= \frac{\mu}{\mu_c}\alpha_k^u a_k^u + \frac{\mu}{\mu_c}m_k^u + \frac{\mu}{\mu_c}e_k^u + \frac{\mu}{\mu_c}\underbrace{\sum_{m=0}^{\mu_c/\mu-1} g_{(k-m\mu K)_{\mu_c K}}\xi^u_{(k-m\mu K)_{\mu_c K}}}_{\triangleq \zeta_k^u\text{, aliased, filtered distortion}} \\ &\qquad + \frac{\mu}{\mu_c}\underbrace{\sum_{m=0}^{\mu_c/\mu-1} g_{(k-m\mu K)_{\mu_c K}}\nu^u_{(k-m\mu K)_{\mu_c K}}}_{\triangleq \vartheta_k^u\text{, aliased, filtered white noise}} \\ &= \frac{\mu}{\mu_c}\left[\alpha_k^u a_k^u + m_k^u + e_k^u + \zeta_k^u + \vartheta_k^u\right], \end{aligned} \tag{4.12}$$

where, for IDAP, α_k^u is equal to $c_x^{(i_f)}$, and the multi-user interference term m_k^u is zero, whereas they are defined as in (4.9) for ZF. The terms in the summation constituting ϑ_k^u are $\frac{\mu_c}{\mu}$ independent Gaussian random variables, $\frac{\mu_c}{\mu}-1$ of which have $\epsilon^2 N_o$ variance and one of which has a variance of N_o. Therefore, ϑ_k^u is a Gaussian random variable with variance $((\frac{\mu_c}{\mu}-1)\epsilon^2+1)N_o$, $\forall k$. That leads to an SINR expression for the k^{th} subcarrier of the u^{th} user for IDAP and ZF as follows:

$$\begin{aligned} SINR_k^u &= \frac{|\alpha_k^u|^2 E\left[|a_k^u|^2\right]}{E\left[|m_k^u|^2\right] + E\left[|e_k^u|^2\right] + E\left[|\zeta_k^u|^2\right] + E\left[|\vartheta_k^u|^2\right]} \\ &= \frac{|\alpha_k^u|^2}{\underbrace{\sum_{l=1,l\neq u}^{U}|\alpha_k^l|^2}_{E\left[|m_k^u|^2\right]} + \underbrace{\left[\mathbf{\Omega}_k^H \mathbf{C}_{\boldsymbol{\eta}_k}\mathbf{\Omega}_k\right]_{u,u}}_{E\left[|e_k^u|^2\right]} + \underbrace{\sum_{m=0}^{\mu_c/\mu-1} g_{k''}^2[\overset{\smile}{\mathbf{\Lambda}}_{k'}^H \mathbf{C}_{\overset{\smile}{\mathbf{y}}_{k'}}\overset{\smile}{\mathbf{\Lambda}}_{k'}]_{u,u}}_{E\left[|\zeta_k^u|^2\right],\ k'=(k-\Delta f-m\mu K)_{\mu_c K}} + E\left[|\vartheta_k^u|^2\right]}, \end{aligned} \tag{4.13}$$

where $E\left[|a_k^u|^2\right]=1$, $k''=(k-m\mu K)_{\mu_c K}$, $E\left[|\vartheta_k^u|^2\right]=((\frac{\mu_c}{\mu}-1)\epsilon^2+1)N_o$, $E\left[|m_k^u|^2\right]$ is MUI power and non-zero only for ZF, and $\alpha_k^u = c_x^{(i_f)}$ for IDAP. Moreover, $\mathbf{C}_{\boldsymbol{\eta}_k}$ and $\mathbf{C}_{\overset{\smile}{\mathbf{y}}_{k'}}$ are the covariance matrices for the quantization distortion from BS_1 and the signal transmitted by BS_2. For IDAP, $\mathbf{C}_{\boldsymbol{\eta}_k}$ can be written as

$$\mathbf{C}_{\boldsymbol{\eta}_k} = E\left[(\boldsymbol{\eta}_k^{(i_f-1)} - \widehat{\boldsymbol{\eta}}_k^{(i_f-1)})(\boldsymbol{\eta}_k^{(i_f-1)} - \widehat{\boldsymbol{\eta}}_k^{(i_f-1)})^H\right], \tag{4.14}$$

whereas for ZF $\mathbf{C}_{\boldsymbol{\eta}_k} = E\left[\boldsymbol{\eta}_k\boldsymbol{\eta}_k^H\right]$. On the other hand, $\mathbf{C}_{\overset{\smile}{\mathbf{y}}_{k'}} = E\left[\overset{\smile}{\mathbf{y}}_{k'}\overset{\smile}{\mathbf{y}}_{k'}^H\right]$ is non-zero only for the first and last $\mu K/2$ entries in terms of k' for both IDAP and ZF, and

expanding it for ZF we get the following equation as

$$\mathbf{C}_{\breve{\overline{\mathbf{y}}}_{k'}} = E\left[\overline{\mathbf{A}}^{ZF}\breve{\overline{\mathbf{x}}}_{k'}^{ZF}(\breve{\overline{\mathbf{x}}}_{k'}^{ZF})^{H}(\overline{\mathbf{A}}^{ZF})^{H} + \breve{\overline{\boldsymbol{\eta}}}_{k'}^{ZF}(\breve{\overline{\boldsymbol{\eta}}}_{k'}^{ZF})^{H}\right] = \overline{\mathbf{A}}^{ZF}\mathbf{C}_{\breve{\overline{\mathbf{x}}}_{k'}}^{ZF}(\overline{\mathbf{A}}^{ZF})^{H} + \mathbf{C}_{\breve{\overline{\boldsymbol{\eta}}}_{k'}}^{ZF}, \tag{4.15}$$

where $\mathbf{C}_{\breve{\overline{\boldsymbol{\eta}}}_{k'}}^{ZF}$ is covariance matrix for the distortion in the transmitted signal $\breve{\overline{\mathbf{y}}}_{k'}$ from BS_2, and $\overline{\mathbf{A}}^{ZF}$ is the associated Bussgang gain matrix due to (4.6). Matrix $\overline{\mathbf{A}}^{ZF}$ can be found as in (4.7), by replacing $\mathbf{C}_{\mathbf{x}_k}$ with $\mathbf{C}_{\breve{\overline{\mathbf{x}}}_{k'}}^{ZF} = E\left[\breve{\overline{\mathbf{x}}}_{k'}^{ZF}(\breve{\overline{\mathbf{x}}}_{k'}^{ZF})^{H}\right]$, which can be written as

$$\mathbf{C}_{\breve{\overline{\mathbf{x}}}_{k'}}^{ZF} = \begin{cases} (c_x^{ZF})^2\mathbf{W}_{k'}^{ZF}(\mathbf{W}_{k'}^{ZF})^{H} \text{ if } k' \in \{0,...,\frac{K}{2}-1\}\bigcup\{\mu_c K - \frac{K}{2},...,\mu_c K - 1\}, \\ \mathbf{0}_{N_t\times N_t} \text{ elsewhere,} \end{cases} \tag{4.16}$$

due to (4.4). In the SINR expression in (4.13), $E\left[|e_k^u|^2\right]$ is the residual distortion power of the in-band subcarriers coming from BS_1 due to quantization, on which ZF precoder has no control, but it can be minimized by IDAP. $E\left[|\zeta_k^u|^2\right]$ is the interference coming from BS_2, on which ZF precoder has no control, but it can be minimized by utilizing IDAP on overlapping OOB subcarriers. $E\left[|\vartheta_k^u|^2\right]$ is the white noise power. Only unkowns in the SINR expression (4.13) are $\mathbf{C}_{\boldsymbol{\eta}_k}$ and $\mathbf{C}_{\overline{\mathbf{y}}_{k'}}$ which can both be found through numerical Monte-Carlo simulations. For ZF precoding in both BS_1 and BS_2 and for large U, it can be shown that $\mathbf{C}_{\boldsymbol{\eta}_k} \approx \mathbf{C}_{\overline{\boldsymbol{\eta}}_{k'}}^{ZF}$ and $\mathbf{C}_{\boldsymbol{\eta}_k}$ is approximately a constant diagonal matrix. In this case, calculation of (4.13) boils down the estimation of only a single scalar parameter in the constant diagonal entries of $\mathbf{C}_{\boldsymbol{\eta}_k}$.

These derivations of the SINR expressions for IDAP and ZF are done for the case of perfect channel. To incorporate channel estimation error, the precoding matrices can be constructed using estimated channel instead of actual channel. For the case of the estimated channel, the rest of the derivation will be similar to the case of the perfect channel. Moreover, to compare experimental results with the SINR expression in (4.13), we have used the analytical expression of SER for M-QAM as follows:

$$SER_k^u = 1 - \left[1 - \frac{2(\sqrt{M}-1)}{\sqrt{M}}\left(1 - \Phi\left(\sqrt{\frac{3SINR_k^u}{M-1}}\right)\right)\right]^2, \tag{4.17}$$

where SER_k^u is the symbol-error-rate for k^{th} subcarrier of u^{th} UE, and M is the QAM order.

4.2 Fully Analytical SINR expression of Quantized ZF for 1-bit DAC

First, we start with computation of $E\left[|e_k^u|^2\right]$ analytically, then countinue with $E\left[|\zeta_k^u|^2\right]$. $\mathbf{e}_k$ is the distortion passed through channel, so $E\left[|e_k^u|^2\right] = \left[\mathbf{\Omega}_k^H \mathbf{C}_{\boldsymbol{\eta}_k} \mathbf{\Omega}_k\right]_{(u,u)}$ ie. the u^{th} diagonal of the covariance matrix of recevied distortion signal. Desired covariance matrix of distortion $\mathbf{C}_{\boldsymbol{\eta}_k}$ in frequency-domain can be computed according to the following proposition.

Proposition 2. $\mathbf{C}_{\boldsymbol{\eta}_k}$ *can be found from* $\mathbf{C}_{\tilde{\boldsymbol{\eta}}}[m]$ *as*

$$\mathbf{C}_{\boldsymbol{\eta}_k} = \mathbf{\Gamma}_k + \mathbf{\Gamma}_k^H - \mathbf{C}_{\tilde{\boldsymbol{\eta}}}[0] \tag{4.18}$$

where $\mathbf{\Gamma}_k = \frac{1}{\mu K} \sum_{m=0}^{\mu K-1} (\mu K - m) \mathbf{C}_{\tilde{\boldsymbol{\eta}}}[m] e^{\frac{-j2\pi mk}{\mu K}}$, $\forall k$, and $\mathbf{C}_{\tilde{\boldsymbol{\eta}}}[m] \triangleq E\left[\tilde{\boldsymbol{\eta}}_n [\tilde{\boldsymbol{\eta}}_{(n-m)}]^H\right]$.

Proof. See Appendix A.2 □

Covariance matrix of time-domain distortion can be found using Bussgang decomposition as

$$\mathbf{C}_{\tilde{\boldsymbol{\eta}}}[m] = \mathbf{C}_{\tilde{\mathbf{y}}}[m] - \mathbf{A}\mathbf{C}_{\tilde{\mathbf{x}}}[m]\mathbf{A}^H \tag{4.19}$$

where $\mathbf{C}_{\tilde{\mathbf{y}}}[m] \triangleq E\left[\tilde{\mathbf{y}}_n \tilde{\mathbf{y}}_{(n-m)}^H\right]$ is the DAC output and $\mathbf{C}_{\tilde{\mathbf{x}}}[m] \triangleq E\left[\tilde{\mathbf{x}}_n \tilde{\mathbf{x}}_{(n-m)}^H\right]$ is the DAC input time-domain covariance matrix for the m^{th} delay. Next, we define $\mathbf{C}_{\mathbf{x}_k} \triangleq E[\mathbf{x}_k \mathbf{x}_k^H]$. Since $E[\mathbf{x}_k \mathbf{x}_{k'}^H] = \mathbf{0}_{N_t \times N_t}$ for $k \neq k'$, $\mathbf{C}_{\tilde{\mathbf{x}}}[m]$ can be found by the following proposition.

Proposition 3. $\mathbf{C}_{\tilde{\mathbf{x}}}[m]$ *can be found from* $\mathbf{C}_{\mathbf{x}_k}$ *as*

$$\mathbf{C}_{\tilde{\mathbf{x}}}[m] = \frac{1}{\mu K} \sum_{k=0}^{\mu K-1} \mathbf{C}_{\mathbf{x}_k} e^{\frac{j2\pi mk}{\mu K}} \tag{4.20}$$

where frequency domain DAC input signal's covariance for ZF is $\mathbf{C}_{\mathbf{x}_k} = (c_x)^2 \mathbf{W}_k \mathbf{W}_k^H$ from (4.4).

Proof. See Appendix A.3 □

Also, by using arc-sine law [37], DAC output's covariance can be found as

$$\begin{aligned}\mathbf{C}_{\tilde{\mathbf{y}}}[m] =& \frac{c_y^2\Delta^2}{\pi}[\text{asin}(\mathbf{D}_{\tilde{\mathbf{x}}}^{-\frac{1}{2}}\Re(\mathbf{C}_{\tilde{\mathbf{x}}}[m])\mathbf{D}_{\tilde{\mathbf{x}}}^{-\frac{1}{2}})] \\ &+ j\ \text{asin}(\mathbf{D}_{\tilde{\mathbf{x}}}^{-\frac{1}{2}}\Im(\mathbf{C}_{\tilde{\mathbf{x}}}[m])\mathbf{D}_{\tilde{\mathbf{x}}}^{-\frac{1}{2}})\end{aligned} \tag{4.21}$$

where $\mathbf{D}_{\tilde{\mathbf{x}}} = \text{diag}(\mathbf{C}_{\tilde{\mathbf{x}}}[0])$. On the other hand, $\boldsymbol{\zeta}_k$ is circularly shifted replica of the received interfering signal after applying IF filter as $E\left[|\zeta_k^u|^2\right] = \sum_{m=0}^{\mu_c/\mu-1} g^2_{(k-m\mu K)_{\mu_c K}} E[|\xi^u_{(k-m\mu K)_{\mu_c K}}|^2] = \sum_{m=0}^{\mu_c/\mu-1} g^2_{(k-m\mu K)_{\mu_c K}} [\breve{\overline{\mathbf{\Lambda}}}_{k'}^H \mathbf{C}_{\breve{\overline{\mathbf{y}}}_{k'}} \breve{\overline{\mathbf{\Lambda}}}_{k'}]_{u,u},\ k' = (k - \Delta f - m\mu K)_{\mu_c K}$. $\mathbf{C}_{\breve{\overline{\mathbf{y}}}_{k'}}$ is the covariance matrix of the BS_2's DAC output at the sampling rate of $\frac{\mu_c}{\mu}F_s$ which can be found from its version at the receiver sampling rate F_s as

$$\mathbf{C}_{\breve{\overline{\mathbf{y}}}_{k'}} = \begin{cases} \mathbf{C}_{\overline{\mathbf{y}}_{k'}} \text{ if } k' \in \{0, ..., \mu K/2 - 1\} \\ \mathbf{C}_{\overline{\mathbf{y}}_{k'}} \text{ if } k' \in \{\mu_c K - \mu K/2, ..., \mu_c K - 1\} \\ \mathbf{0}_{N_t \times N_t} \text{ elsewhere.} \end{cases} \tag{4.22}$$

DAC output covariance matrix in frequency domain at the receiver sampling rate $\mathbf{C}_{\overline{\mathbf{y}}_{k'}}$ can be found using Proposition 2 as

$$\mathbf{C}_{\overline{\mathbf{y}}_{k'}} = \overline{\mathbf{\Gamma}}_{k'} + \overline{\mathbf{\Gamma}}_{k'}^H - \mathbf{C}_{\tilde{\overline{\mathbf{y}}}}[0] \tag{4.23}$$

where $\overline{\mathbf{\Gamma}}_{k'} = \frac{1}{\mu K}\sum_{m=0}^{\mu K-1}(\mu K - m)\mathbf{C}_{\tilde{\overline{\mathbf{y}}}}[m]e^{\frac{-j2\pi mk'}{\mu K}},\ \forall k'$, and $\mathbf{C}_{\tilde{\overline{\mathbf{y}}}}[m]$ is the covariance matrix of the DAC output of 2^{nd} BS for m^{th} delay found by using (4.21) with $\mathbf{x}_k$ being DAC input of 2^{nd} BS.

4.3 Fully Analytical SINR expression of Quantized ZF for multi-bit DAC

Same as one-bit DAC case, we need to find distortion covariance matrice of BS_1 namely $\mathbf{C}_{\boldsymbol{\eta}_k}$ and DAC output covariance matrice of BS_2 namely $\mathbf{C}_{\overline{\mathbf{y}}_{k'}}$. We will start by finding DAC input covariance matrix in frequency domain $\mathbf{C}_{\mathbf{x}_k}$ and work our way up to $\mathbf{C}_{\boldsymbol{\eta}_k}$. $\mathbf{C}_{\mathbf{x}_k} = c_x^2\mathbf{W}_k\mathbf{W}_k^H$ and $\mathbf{A}$ is found using (4.7) with the desired number of bits, q. Then, time-domain DAC input covariance found as in (4.20). Now, we need an analytical expression for the DAC output covariance matrix like in the case of 1-bit, however there is no closed form expression. Therefore, we will make an assumption that only diagonal entries of $\mathbf{C}_{\tilde{\mathbf{y}}}[0]$ are non-zero, so u^{th} diagonal entry of

$\mathbf{C}_{\tilde{\mathbf{y}}}[0]$, by dropping ZF superscript, can be found as

$$\begin{aligned}\left[\mathbf{C}_{\tilde{\mathbf{y}}}[0]\right]_{(u,u)} =& 2\sum_{i=0}^{L-1} l_i^2 \mathbb{P}[b_i < \Re(\widetilde{x}_0^u) < b_{i+1}] \\ =& 2\sum_{i=0}^{L-1} l_i^2 [\Phi(\sqrt{2}b_{i+1}/\sigma_{\widetilde{x}_0^u}) - \Phi(\sqrt{2}b_i/\sigma_{\widetilde{x}_0^u})]\end{aligned} \tag{4.24}$$

where $\sigma^2_{\widetilde{\mathbf{x}}_0^u}$ is the u^{th} diagonal of the $\left[\mathbf{C}_{\tilde{\mathbf{x}}}[0]\right]_{(u,u)}$, i.e. quantizer input of power the u^{th} antenna. Now, we can find distortion covariance matrix in time-domain as

$$\mathbf{C}_{\tilde{\boldsymbol{\eta}}}[0] = \mathbf{C}_{\tilde{\mathbf{y}}}[0] - \mathbf{A}\,\mathrm{diag}(\mathbf{C}_{\tilde{\mathbf{x}}}[0])[\mathbf{A}]^H \tag{4.25}$$

Here, $\mathbf{C}_{\tilde{\boldsymbol{\eta}}}[m]$ is assumed to be close to zero for $m \neq 0$, meaning distortion sequence at different samples has a negligeable effect on each other. Finally, distortion covariance matrice in frequency domain can be found using Proposition 2 as

$$\mathbf{C}_{\boldsymbol{\eta}_k} = \boldsymbol{\Gamma}_k + \boldsymbol{\Gamma}_k^H - \mathbf{C}_{\tilde{\boldsymbol{\eta}}}[0] = \mathbf{C}_{\tilde{\boldsymbol{\eta}}}[0] \tag{4.26}$$

where $\boldsymbol{\Gamma}_k = \frac{1}{\mu K}\sum_{m=0}^{\mu K-1}(\mu K - m)\mathbf{C}_{\tilde{\boldsymbol{\eta}}}[m]e^{\frac{-j2\pi mk}{\mu K}} = \mathbf{C}_{\tilde{\boldsymbol{\eta}}}[0],\ \forall k$. Then, as in the case of one-bit DACs, $E\left[|e_k^u|^2\right]$ and $E\left[|\zeta_k^u|^2\right]$ is found by using $\mathbf{C}_{\boldsymbol{\eta}_k}$ and $\mathbf{C}_{\overline{\mathbf{y}}_{k'}}$ for multi-bit SINR expression.

CHAPTER 5

NUMERICAL RESULTS

In this chapter, we present a comprehensive performance evaluation of our proposed precoder IDAP, along with the benchmark precoder SQUID and ZF precoder. The evaluation is conducted through Monte Carlo simulations, focusing on key performance metrics such as bit-error rate (BER), symbol-error rate (SER), and power-spectral density (PSD). To begin, we analyze the performance of the precoders in a scenario where a single BS serves its users. This initial analysis provides insights into the precoders' performance in a non-interfering environment, and demonstrates how well they reduce the in-band quantization distortion. Subsequently, we extend our investigation by introducing a second BS, allowing us to examine the precoders' performance under interference conditions. By considering the effects of interference, we gain a deeper understanding of how the precoders handle challenging scenarios. Through our comprehensive Monte Carlo simulations, we aim to provide a thorough evaluation of the performances of IDAP, SQUID, and ZF precoders, enabling a comprehensive comparison in terms of BER, SER, and PSD.

5.1 Downlink Scenario for Single BS

Our performance metrics include uncoded and coded BER, uncoded SER, as well as out-of-band (OOB) emissions or PSD of the transmitted signals. We compare the proposed precoder IDAP with linear quantized oversampled ZF precoder and the precoder introduced in [14], which constitute comparable complexity benchmark precoders. Our results demonstrate that IDAP outperforms both the linear ZF precoder and the precoder in [14] in terms of error rate and/or OOB emissions performance.

Additionally, we include ideal unquantized ZF precoder as a benchmark to observe the limit how much IDAP can mitigate quantization distortion. In the BER and SER plots, the horizontal axis values represent the received signal-to-noise ratio (Rx SNR) per user and per active subcarrier, which is given by $E\left[|\left|[\mathbf{\Omega}_k^H \mathbf{y}_k]_u\right|^2\right]/N_o, \forall u$. The number of active subcarriers K is set to 128 for all simulations. We consider two channel scenarios: rich scattering environment without a dominant line-of-sight (LoS) path and another with a LoS path. We model the non-LoS channels as Rayleigh fading and LoS channels as Rician fading channels. The power delay profile (PDP) of the channel follows the COST-207 delay profile for suburban and urban areas [38]. For the Rayleigh fading scenarios, the total number of non-zero multipath components is $5\mu_c$ with $P = 32\mu_c$, which are chosen as uncorrelated in time and space in line with the discussions in [33]. For the Rician fading channel, the parameters are selected as in [2]: the total number of non-zero multipath components is 5, corresponding to a sparse channel, with $P = 32\mu_c$, $\varsigma_u^n = 3^\circ$, φ_u^n is chosen from a uniform distribution between ± 60, except for the first tap where the mean arriving angle selection is repeated if any two mean arriving angles are closer than the angular spread for any user. For the first tap, $r_f = 10$ dB, and for the other taps, $r_f = 3$ dB, as more LOS dominance is present for the first arriving paths. The PDP of the channel again follows the COST-207 delay profile for suburban and urban areas [38]. In scenarios containing channel estimation error, the estimated channel utilized in precoding is denoted with hat as $\widehat{\mathbf{\Omega}}_k^H$, and actual channel is $\mathbf{\Omega}_k^H = \widehat{\mathbf{\Omega}}_k^H + \mathbf{E}_k$ where $\mathbf{E}_k \in \mathbb{C}^{U \times N_t}$ is channel estimation error matrix. Here, we assumed that estimated channel and channel error is uncorrelated, $E\left[\frac{1}{\mu_c K}\sum_{k=0}^{\mu_c K-1} \mathrm{trace}(\widehat{\mathbf{\Omega}}_k^H \widehat{\mathbf{\Omega}}_k)\right] = N_t U$, and each element of $\mathbf{E}_k$ is realized as i.i.d. zero-mean CSCG random variable with variance σ_e^2 for all subcarriers[1]. This makes the power ratio of each element of $\widehat{\mathbf{\Omega}}_k^H$ and $\mathbf{E}_k$ equal to $1/\sigma_e^2$. We have selected σ_e^2 as -16 dB for 1-bit DAC, and -25 dB for 2-bit DAC as achievable values according to [2]. In scenarios involving two base stations, we have $U = U'$. For all simulations where channel coding is employed, the coding scheme employed is rate 3/4 low-density parity check code (LDPC) specified in IEEE-802.11 standard [39]. Unless otherwise stated, N_t =64, μ_c =8. Quant./Qnt. IDAP, Quant./Qnt. ZF and UnQuant./UnQnt. ZF in the plot legends refer to quantized IDAP, quantized and

[1] Here, we have assumed additive white Gaussian noise to model channel estimation error. Depending on the scenario correlated noise models can also be used.

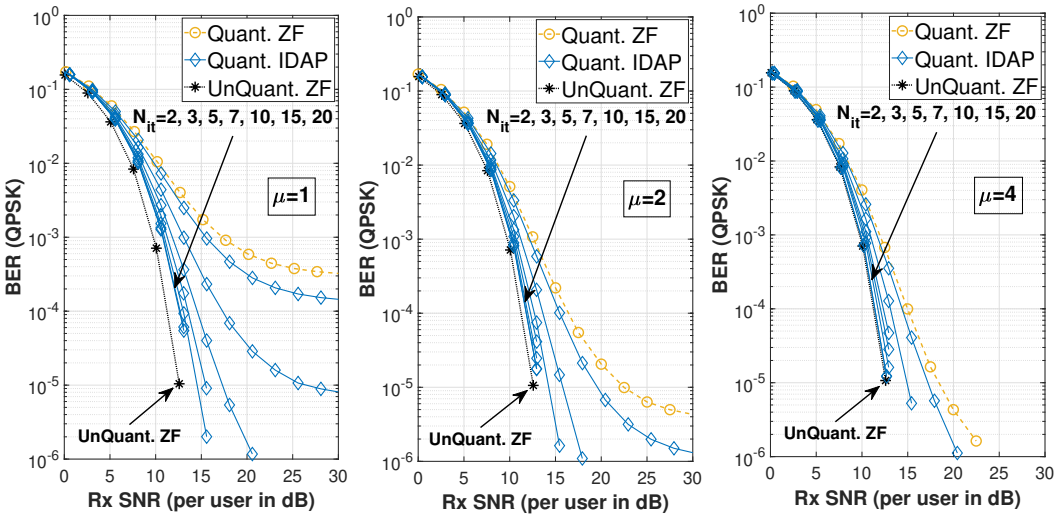

(a) $\mu = 1$ (b) $\mu = 2$ (c) $\mu = 4$

Figure 5.1: BER vs Rx SNR for $N_t = 128$, U=16, QPSK, $q = 1$, various N_{it}.

unquantized linear ZF, respectively. The analytical performance curves are plotted according to (4.13) and (4.17).

Fig. 5.1 shows the error-rate performance of IDAP for different N_{it} values to observe its convergence rate. Since OOB supression is not required here, IDAP takes $\mathcal{S}_{ov}$ as an empty set. The results show that when the oversampling factor is increased, IDAP converges faster, as seen in the case of $Nt = 128$, $U = 16$, QPSK, and 1-bit DAC.

In Fig. 5.2, we illustrate the error-rate performance of IDAP for various N_{it} and μ as in Fig. 5.1, but for a higher load, 16-QAM to observe the necessary number of iterations for the convergence of IDAP when constellation contains more symbols. While the necessary number of iterations for convergence is relatively large for no oversampling, 15 iterations seem to be enough for higher oversampling factors of μ =2 or μ =4, as shown in Fig. 5.2b and Fig. 5.2c.

To examine the OOB radiation performances, Fig. 5.3a shows the PSD at the user side of quantized SQUID [14], quantized ZF, and quantized IDAP for various oversampling factors. To achieve suppression throughout the whole OOB region $\mathcal{S}_o$, IDAP takes the OOB suppression region $\mathcal{S}_{ov} = \mathcal{S}_o$. If the PSD values at the OOB close to the in-band portion of the spectrum are compared, quantized SQUID and quantized

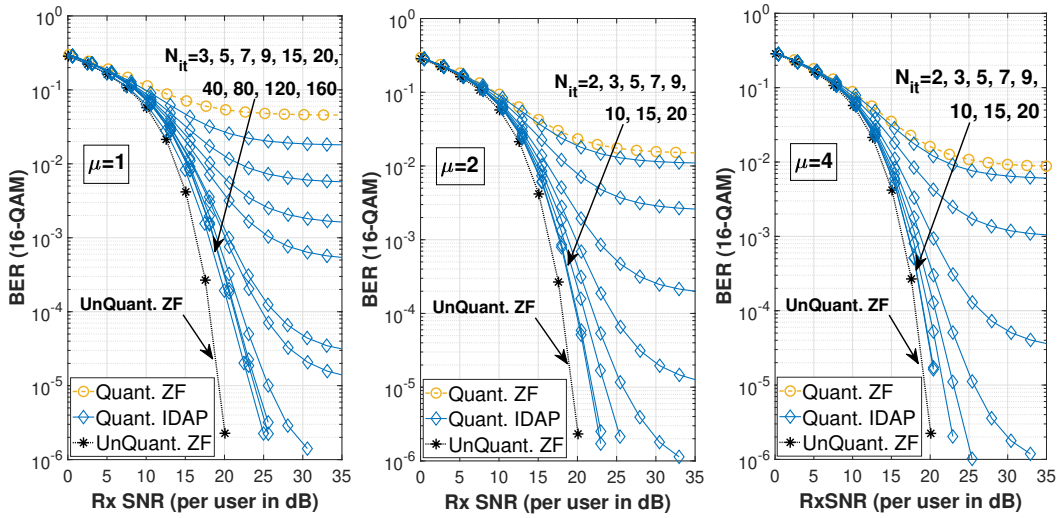

(a) μ =1 (b) μ =2 (c) μ =4

Figure 5.2: BER vs Rx SNR for N_t =128, U =16, 16-QAM, q =1, various N_{it}.

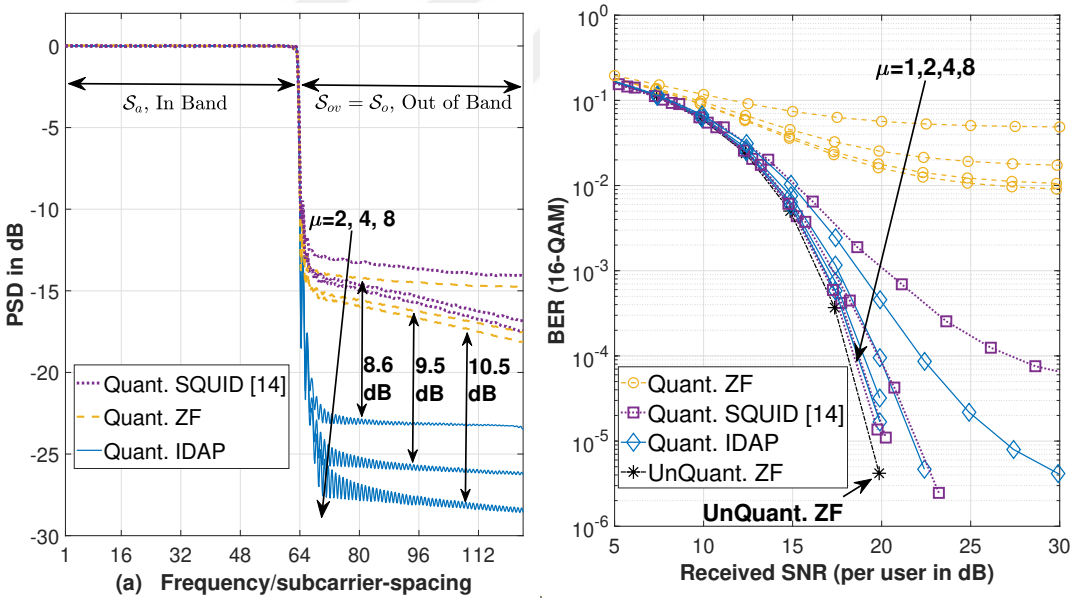

(a) PSD (b) BER vs Rx SNR

Figure 5.3: N_t =64, U =8, 16-QAM, q =1, N_{it} =40, μ =1, 2, 4, 8 for IDAP and SQUID. A tapered cosine window function with 0.25 tapers is applied on transmit waveforms.

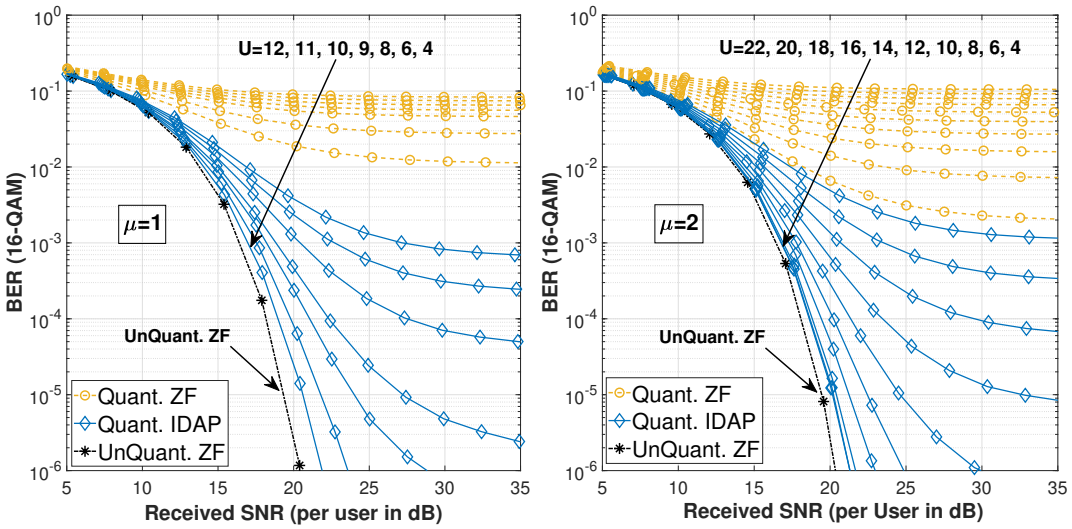

(a) $\mu = 1$ (b) $\mu = 2$

Figure 5.4: BER vs Rx SNR for $N_t = 64$, 16-QAM, $q = 1$, $N_{it} = 80$ various U for IDAP and ZF.

ZF have similar PSD, with SQUID being slightly worse. This is because SQUID focuses on minimizing in-band distortion to improve BER and does not prioritize reducing distortion in OOB. In contrast, IDAP cancels out a significant amount of OOB distortion, resulting in lower OOB radiation compared to SQUID and quantized ZF, providing up to 10.5 dB OOB PSD difference achieved at μ =8. The error-rate performances for the same simulation setting are also compared in Fig. 5.3b, where IDAP and SQUID show superior performance compared to quantized ZF. At high oversampling values, IDAP and SQUID perform close to unquantized ZF. For μ =1, IDAP outperforms SQUID, providing about 5 dB SNR advantage for the BER level of 10^{-4}. Therefore, it can be concluded that IDAP outperforms SQUID (for μ =1) and quantized ZF in terms of BER and provides much lower OOB emissions compared to SQUID and quantized ZF for any oversampling factor.

Fig. 5.4 shows how IDAP and ZF perform under varying user loads for $N_t = 64$, 16-QAM, $q = 1$. Quantized IDAP clearly outperforms quantized ZF and perform closer unquantized ZF for smaller U values. IDAP at $\mu = 2$, has almost twice the user load capacity compared to $\mu = 1$ for similar BER values. This indicates that higher oversampling factors can support much more users.

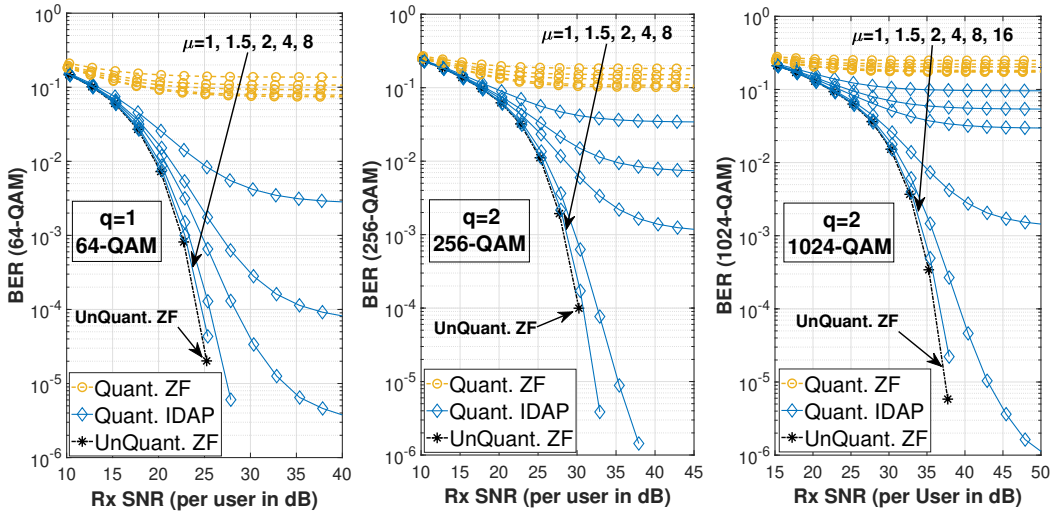

(a) q =1, 64-QAM (b) q =2, 256-QAM (c) q =2, 1024-QAM

Figure 5.5: BER vs Rx SNR for N_t =64, U =8, various μ.

The effect of oversampling factor for various number of quantizer bits and modulation orders are also investigated in Fig. 5.5 for U =8. It seems that quantized ZF does not benefit from higher oversampling factors, while the performance of IDAP improves a lot with increasing oversampling factors, and outperforms quantized ZF. Noted from Fig. 5.5b and Fig. 5.5c, IDAP can accommodate modulation orders as large as 64-QAM with 1-bit DACs and 1024-QAM with 2-bit DACs, for moderate to high oversampling rates. Interested reader may also refer to the conference version of this paper [40] to see the robustness of IDAP to various user loads.

Fig. 5.6 illustrates the error-rate performance of IDAP and SQUID under Rayleigh fading for the 1-bit, 64-QAM case with $N_t = 64$ and $U = 12$ for various values of μ. As μ increases, the BER performance of both IDAP and SQUID improves for both coded and uncoded cases. IDAP outperforms SQUID for all values of μ, with the performance gap being greater at lower μ values. While coding significantly reduces the need for high oversampling factors, increasing the oversampling factor is still highly advantageous.

To observe the performances of the precoders under examination in Rician Fading channels, error-rate performances are obtained as presented in Fig. 5.7 for 1-bit DAC, 64-QAM, U =12 and various oversampling factors. As can be noted in Fig. 5.7, as

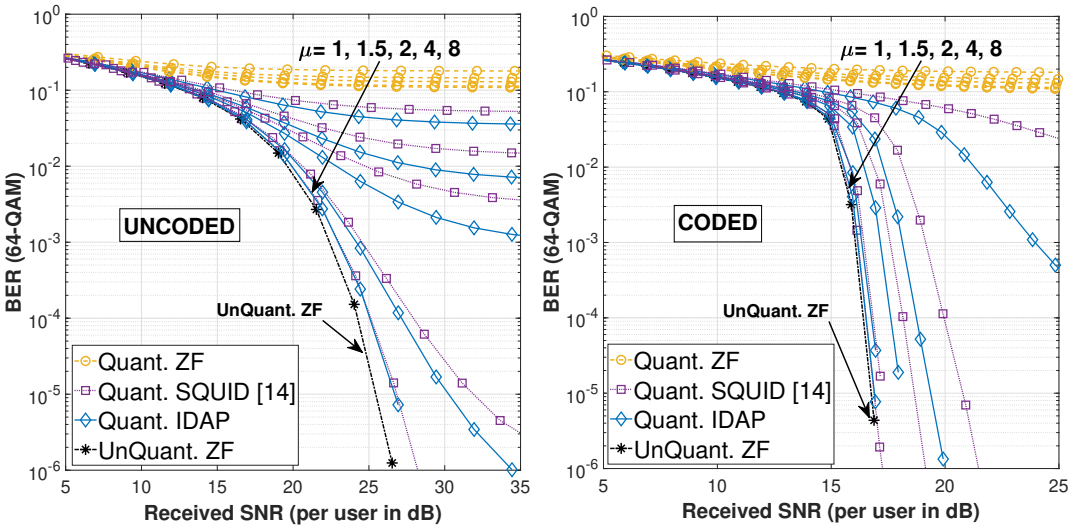

(a) Uncoded BER (b) Coded BER

Figure 5.6: BER vs Rx SNR for $N_t = 64$, U=12, q=1, 64-QAM, various μ, Rayleigh channel.

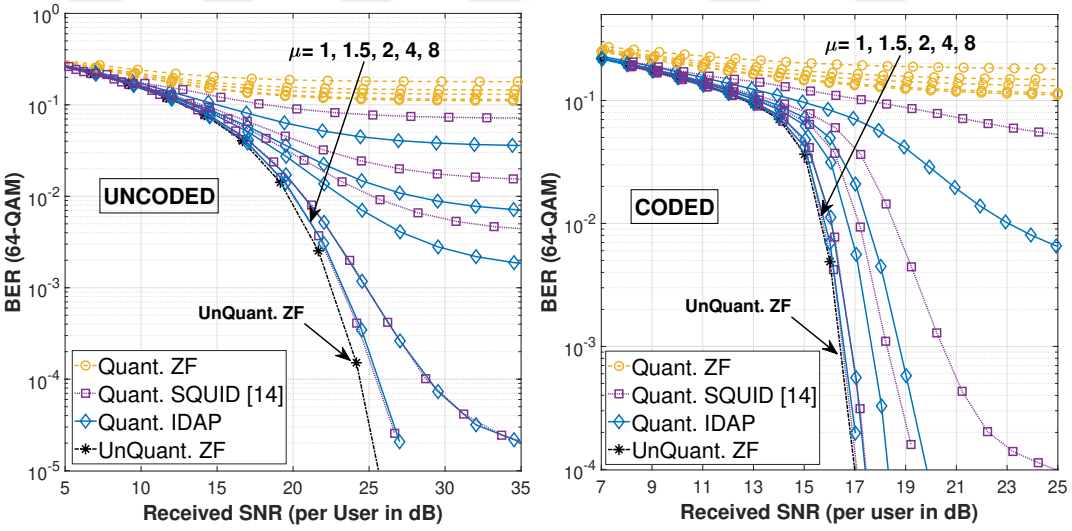

(a) Uncoded BER (b) Coded BER

Figure 5.7: BER vs Rx SNR for N_t =64, U =12, q =1, 64-QAM, various μ, Rician channel.

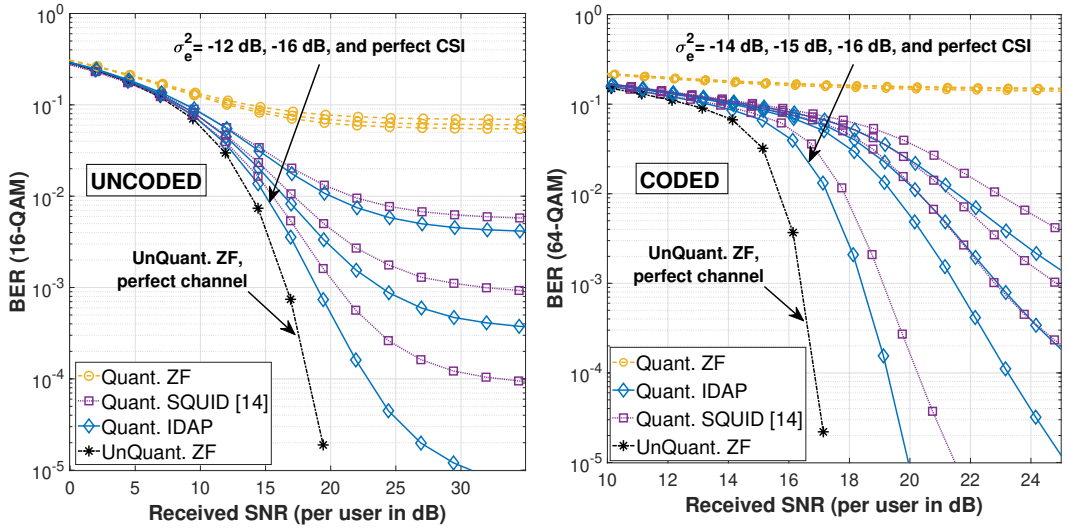

(a) U =12, 16-QAM, Uncoded BER

(b) U =11, 64-QAM, Coded BER

Figure 5.8: BER vs Rx SNR for N_t =64, q =1, μ =1.5 Rician channel.

μ increases, both IDAP and SQUID demonstrate an improvement in BER for coded and uncoded cases. However, IDAP consistently outperforms SQUID for all μ values, with a more significant performance gap observed at lower μ values. Although coding reduces the need for high oversampling factors, increasing the oversampling factor still seems to be beneficial.

Fig. 5.8 shows the error-rate performance of IDAP and SQUID under Rician fading and channel estimation errors. For both uncoded and coded cases, channel estimation error is indicated on the texted arrow such as -16 dB. For both uncoded and coded cases, q =1 and μ =1.5. For the uncoded case, IDAP has a clear advantage over SQUID for both perfect and imperfect channel-state information (CSI) cases. For the coded case, IDAP again outperforms SQUID. Like in the uncoded case, IDAP's performance drops as channel estimation error increases, yet it is always superior to quantized ZF and SQUID. Moreover, it seems that desired BER levels can be achieved by increasing the SNR unlike the uncoded case where error-floors are observed.

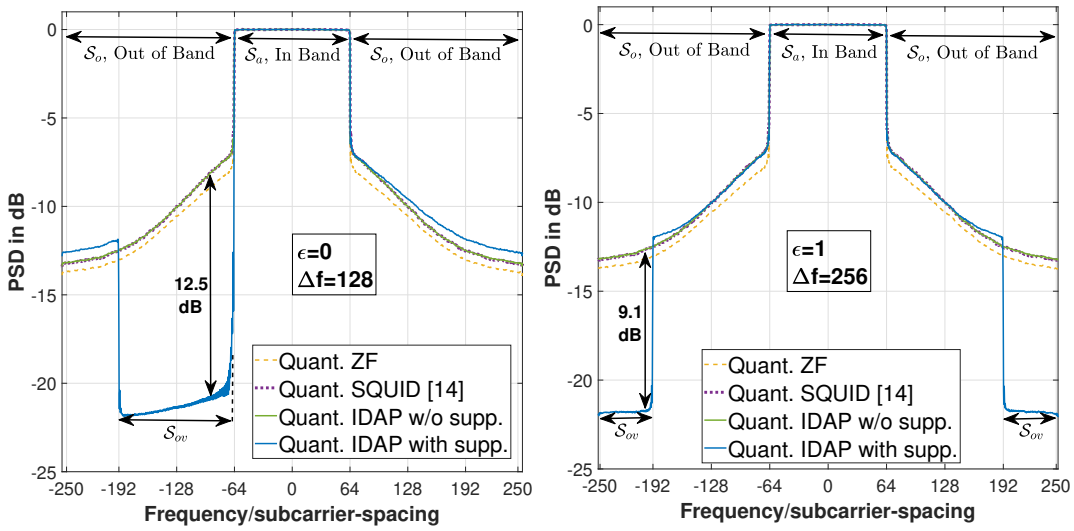

(a) ϵ =0 , Δf =128

(b) ϵ =1 , Δf =256

Figure 5.9: PSD for N_t =64, U =8, q =1, 16-QAM, μ =4.

5.2 Interfering Adjacent Band Scenario for Multiple BSs

In this section, we present simulations performed for the case of multiple base stations operating at adjacent channel bands and interfering with each other due to aliasing. The interfering band channel is created with the same parameters (same PDP, fading type) as the desired channel band. Fig. 5.9 presents the PSD of the received interfering signal coming from BS_2 to a user served by BS_1 for U =8, q =1, 16-QAM, μ =4. For ϵ =0, Δf =128 case, all of the in-band of the intented user is directly hit by the interfering signal from BS_2, whereas for ϵ =1, Δf =256 case, half of the in-band signal is directly hit and the other half is hit due to aliasing of BS_2 signal which is visualized in Fig. 4.1. In Fig. 5.9, the precoder named as "IDAP with supp." suppresses OOB radiation by precoding at the subcarriers of $\mathcal{S}_{ov}$, where it will hit the in-band of the users served by BS_1, whereas the precoder referred to as "IDAP without supp." chooses $\mathcal{S}_{ov}$ as empty set which makes $\mathbf{x}_k = \mathbf{0}_{N_t}$ for all OOB region. IDAP with suppression significantly reduces OOB emission throughout the overlapping frequency bins up to 12.5 dB better compared to SQUID, IDAP without suppression and Quant. ZF for ϵ =0, Δf =128 case. This advantage is about 9.1 dB for ϵ =1, Δf =256 case.

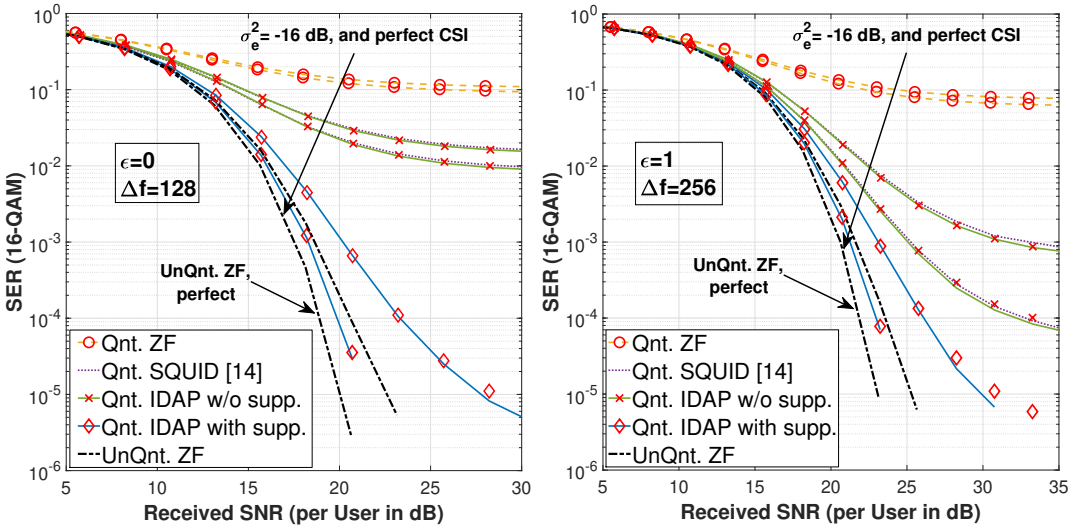

(a) ϵ =0 , Δf =128 (b) ϵ =1 , Δf =256

Figure 5.10: SER vs Rx SNR for N_t =64, U =8, q =1, 16QAM, μ =4, perfect/imperfect CSI. Red markers are analytical SER values, and lines are experimental SER values.

Fig. 5.10 presents the error-rate performances for the same simulation parameters as selected in Fig. 5.9. While SQUID and IDAP without suppression performs almost same, IDAP with suppression, outperforms both SQUID and quantized ZF significantly, with a higher performance gap for ϵ =0, Δf =128 compared to the case ϵ =1, Δf =256, both under perfect and imperfect CSI conditions. It should be noted that the performance gap between IDAP and SQUID was much smaller for μ =4, when there were no interfering BS. Thus, interfering BS scenario further emphasizes the importance of OOB emission reduction achieved by IDAP. Also, our analytical SER results, which are indicated with red markers, coincides with experimental SER's as red markers overlap with the lines for both perfect and imperfect CSI. At this point, one might ask why IDAP without suppression doesn't perform better than SQUID since that was the case for single BS scenario. The answer is that although IDAP without suppression reduces in-band distortion better than SQUID, OOB distortion is the dominant distortion that decides SER for multiple BS scenario, and both IDAP without suppression and SQUID have the same PSD levels in OOB. SNR gap between IDAP with suppression and unquantized ZF is increased for imperfect CSI compared

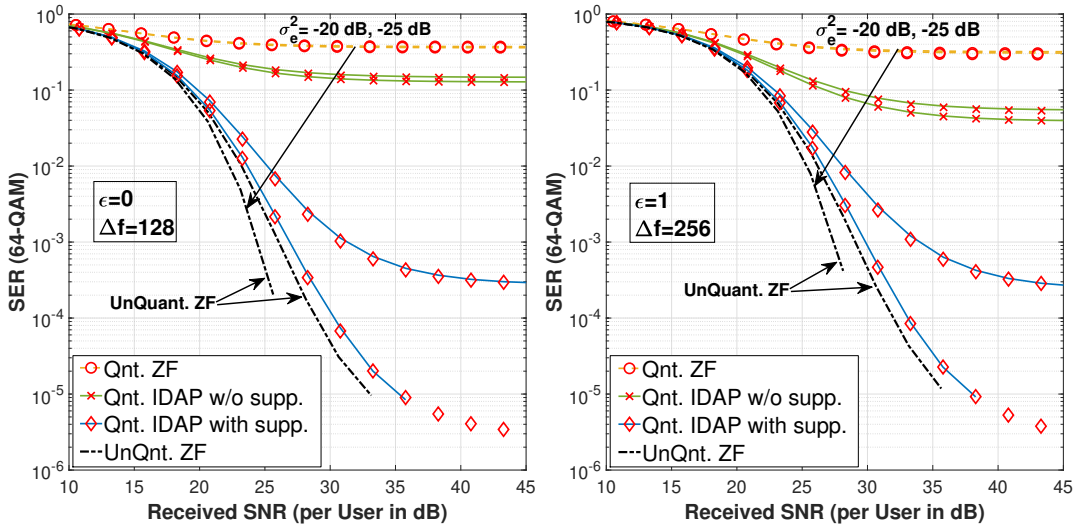

(a) ϵ =0 , Δf =128 (b) ϵ =1 , Δf =256

Figure 5.11: SER vs Rx SNR for N_t =64, U =8, q =2, 64-QAM, μ =4, for -25 dB and -20 dB channel estimation error. Red markers are analytical values, and lines are experimental values.

to perfect CSI, because unquantized ZF suffers only from in-band distortion of BS_1, whereas IDAP as well as SQUID and quantized ZF have interference coming from BS_2 on top of in-band distortion from BS_1.

Fig. 5.11 shows how the precoding schemes work under different channel estimation quality for U =8, q =2, 64-QAM, μ =4. It shows that OOB suppression is meaningful even under channel estimation error and multi-bit quantization when IDAP with suppression is compared to IDAP without suppression. Also, analytical SER values, indicated with red markers, are in consistency with the simulated values.

Fig. 5.12 presents the received signal PSD for U =8, 64-QAM, μ =4 for various q. It shows that IDAP suppresses OOB emisson for q =1, 2, 3, which is remarkable even when q =3.

As the final simulation, Fig. 5.13 illustrates the error-rate performances for various number of quantizer bits. It can be noted that IDAP with suppression exhibits superior performance for all quantizer resolutions compared to quantized ZF. SQUID cannot be included in the plots, as it is not designed for multi-bit multi-amplitude quantiz-

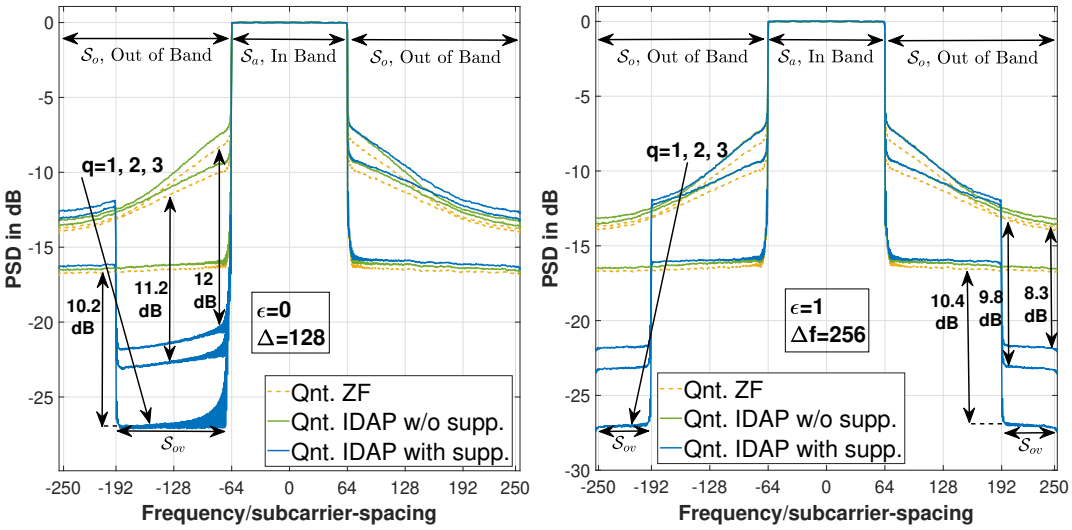

(a) ϵ =0 , Δf =128 (b) ϵ =1 , Δf =256

Figure 5.12: PSD for N_t =64, U =8, various q, 64-QAM, μ =4.

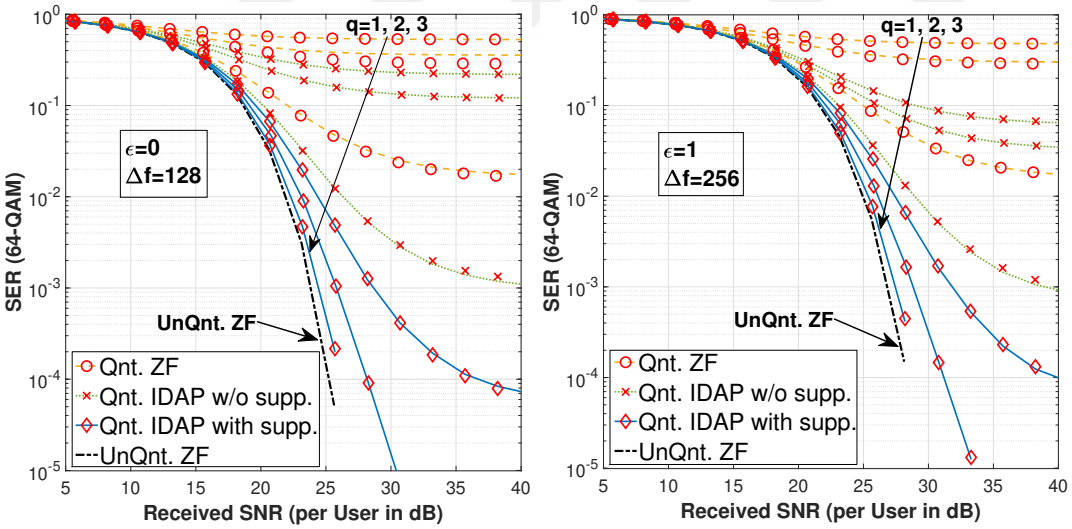

(a) ϵ =0 , Δf =128 (b) ϵ =1 , Δf =256

Figure 5.13: SER vs Rx SNR for N_t =64, U =8, various q, 64-QAM, μ =4, perfect channel. Red markers are analytical SER values, and lines are experimental SER values.

ers. Fig. 5.13 shows that, increasing quantizer bits makes IDAP perform much closer to unquantized ZF. Moreover, analytical results for IDAP coincides well with experimental results, verifying the accuracy of the presented analysis. Since, we didn't make an assumption at q =1 for quantized ZF, there is no mismatch for the analytical and experimental results. Nevertheless, there is a slight mismatch for q =2,3, which is more visible for Δf =128 case. This is due to the assumption we made on deriving the fully analytical SINR expressions. In (4.24), we assumed that the covariance matrix of the DAC output signal to be diagonal. This becomes valid as the spatial correlation among antennas decreases, but the number of bits is not enough for this particular setup which is why at q =2, there is more mismatch than q =3. Also, in (4.25), we assumed that the correlation of the distortion sequence at different time instances can be negligible. This is valid at higher number of bits and lower oversampling factors. Nonetheless, for this setup, q =2, 3 is not enough to make it fully uncorrelated. Also, μ =4 directly increases the correlation at different time instances. This correlation implies that the OOB of the quantized ZF will have a curved shaped, where the PSD decreases as you go further from the inband, which can be seen in Fig. 5.12. However, we assumed it to be uncorrelated, e.g. PSD to be flat at the OOB subcarriers, which may be seen as more valid at the OOB tails, but not so valid at the OOB that is close to inband. This is the reason why there is more mismatch at Δf =128 than Δf =256 case.

CHAPTER 6

CONCLUSIONS

This thesis investigates the effect of quantization, and presents an iterative distortion-aware precoder called IDAP that is applicable to different channel types, modulation orders, DAC bit resolutions, and oversampling values. The precoder outperforms existing benchmark quantized oversampling precoders of comparable complexity in terms of error-rate and OOB emissions. Moreover, IDAP can achieve performance similar to unquantized ideal ZF precoder in practical cases in terms of error-rate which motivates the high capability of our distortion cancellation. As can bee seen from simulation results containing single BS, IDAP has advantage over other precoders in terms of minimizing the in-band distortion which facilitates the improved error-rate performance. Moreover, from simulations containing an interfering BS, we observe that reducing the OOB emission can be so critical that a precoder which has a good error-rate performance in single BS scenario, SQUID, can exhibit very poor error-rate performance when there is interference. On the other hand, IDAP has the ability to suppress OOB emissions in specific OOB locations, minimizing possible adjacent channel interference, while maximizing the error-rate performance by cancelling the non-linear in-band distortion. The OOB reduction advantage of the proposed precoder compared to benchmark precoders can be up to 12 dB in some cases which resulted in significant error-rate performance differences. This can be useful in scenarios where OOB emissions, thus inter-cell interference, are increased due to the nonlinearity introduced by low-resolution DACs employed in massive MIMO arrays. The paper also presents the performance analysis of the proposed IDAP precoder and ZF precoder under interference from a secondary base station. The provided performance analysis is the first to take into account aliasing from adjacent channels for quantized MIMO and provides accurate values close to simulation results.

REFERENCES

[1] T. L. Marzetta, E. G. Larsson, H. Yang, and H. Q. Ngo, *Fundamentals of massive MIMO*. Cambridge, UK: Cambridge Univ. Press, 2016.

[2] A. B. Üçüncü and G. M. Güvensen, "A reduced complexity ungerboeck receiver for quantized wideband massive SC-MIMO," *IEEE Trans. Commun.*, vol. 69, no. 7, pp. 4921–4936, 2021.

[3] S. Jacobsson, G. Durisi, M. Coldrey, and C. Studer, "Linear precoding with low-resolution DACs for massive MU-MIMO-OFDM downlink," *IEEE Trans. Wireless Commun.*, vol. 18, no. 3, pp. 1595–1609, 2019.

[4] A. B. Üçüncü and A. O. Yılmaz, "Sequential linear detection in one-bit quantized uplink massive MIMO with oversampling," in *2018 IEEE 88th Vehicular Technology Conference (VTC-Fall)*, 2018, pp. 1–5.

[5] S. Jacobsson, G. Durisi, M. Coldrey, T. Goldstein, and C. Studer, "Quantized precoding for massive MU-MIMO," *IEEE Trans. Commun.*, vol. 65, no. 11, pp. 4670–4684, 2017.

[6] L. T. N. Landau and R. C. de Lamare, "Branch-and-bound precoding for multiuser MIMO systems with 1-bit quantization," *IEEE Wireless Commun. Lett.*, vol. 6, no. 6, pp. 770–773, 2017.

[7] S. Jacobsson, G. Durisi, M. Coldrey, U. Gustavsson, and C. Studer, "Throughput analysis of massive MIMO uplink with low-resolution ADCs," *IEEE Trans. Wireless Commun.*, vol. 16, no. 6, pp. 4038–4051, 2017.

[8] A. K. Saxena, I. Fijalkow, and A. L. Swindlehurst, "Analysis of one-bit quantized precoding for the multi-user massive MIMO downlink," *IEEE Trans. Signal Process.*, vol. 65, no. 17, pp. 4624–4634, 2017.

[9] A. Tabeshnezhad, A. L. Swindlehurst, and T. Svensson, "Reduced complexity

precoding for one-bit signaling," *IEEE Trans. Veh. Technol.*, vol. 70, no. 2, pp. 1967–1971, 2021.

[10] A. Gokceoglu, E. Björnson, E. G. Larsson, and M. Valkama, "Spatio-temporal waveform design for multi-user massive MIMO downlink with 1-bit receivers," *IEEE J. Sel. Topics Signal Process.*, vol. 11, no. 2, pp. 347–362, 2017.

[11] D. M. V. Melo, L. T. N. Landau, and R. C. de Lamare, "Zero-crossing precoding with maximum distance to the decision threshold for channels with 1-bit quantization and oversampling," in *IEEE Int. Conf. Acoust., Speech and Signal Process. (ICASSP)*, 2020, pp. 5120–5124.

[12] ——, "Zero-crossing precoding with MMSE criterion for channels with 1-bit quantization and oversampling," in *24th Int. ITG Workshop Smart Antennas*, 2020, pp. 1–6.

[13] M. Shao, W.-K. Ma, Q. Li, and A. L. Swindlehurst, "One-bit sigma-delta MIMO precoding," *IEEE J. Sel. Topics Signal Process.*, vol. 13, no. 5, pp. 1046–1061, 2019.

[14] S. Jacobsson, O. Castañeda, C. Jeon, G. Durisi, and C. Studer, "Nonlinear precoding for phase-quantized constant-envelope massive MU-MIMO-OFDM," in *Int. Conf. Telecommun. (ICT)*, 2018, pp. 367–372.

[15] A. Mezghani and R. W. Heath, "Massive MIMO precoding and spectral shaping with low resolution phase-only DACs and active constellation extension," *IEEE Trans. Wireless Commun.*, vol. 21, no. 7, pp. 5265–5278, 2022.

[16] S. Jacobsson, G. Durisi, M. Coldrey, and C. Studer, "Massive MU-MIMO-OFDM downlink with one-bit DACs and linear precoding," in *2017 IEEE Global Commun. Conf.*, 2017, pp. 1–6.

[17] S. Jacobsson, C. Lindquist, G. Durisi, T. Eriksson, and C. Studer, "Timing and frequency synchronization for 1-bit massive MU-MIMO-OFDM downlink," in *IEEE 20th Int. Workshop Signal Process. Adv. Wireless Commun. (SPAWC)*, 2019, pp. 1–5.

[18] J. Choi, D. J. Love, D. R. Brown, and M. Boutin, "Quantized distributed reception for MIMO wireless systems using spatial multiplexing," *IEEE Trans. Signal Process.*, vol. 63, no. 13, pp. 3537–3548, 2015.

[19] K. U. Mazher, A. Mezghani, and R. W. Heath, "Multi-user downlink beamforming using uplink downlink duality with 1-bit converters for flat fading channels," *IEEE Trans. Veh. Technol.*, vol. 71, no. 12, pp. 12 885–12 900, 2022.

[20] M. Bayraktar and G. M. Guvensen, "An efficient interference-aware constrained massive MIMO beamforming for mm-wave JSDM," *IEEE Access*, vol. 9, pp. 87 877–87 897, 2021.

[21] D. Calvetti, L. Reichel, and D. C. Sorensen, "An implicitly restarted lanczos method for large symmetric eigenvalue problems," *Electron. Trans. on Numer. Anal.*, vol. 2, no. 1, p. 21, 1994.

[22] K. U. Mazher, A. Mezghani, and R. W. Heath, "Multi-user downlink beamforming using uplink downlink duality with CEQs for frequency selective channels," 2022. [Online]. Available: https://arxiv.org/abs/2208.01151

[23] A. Mezghani, R. Ghiat, and J. A. Nossek, "Transmit processing with low resolution D/A-converters," in *2009 16th IEEE Int. Conf. on Electronics, Circuits and Syst. - (ICECS 2009)*, 2009, pp. 683–686.

[24] O. B. Usman, H. Jedda, A. Mezghani, and J. A. Nossek, "MMSE precoder for massive mimo using 1-bit quantization," in *2016 IEEE Int. Conf. on Acoust., Speech and Signal Process. (ICASSP)*, 2016, pp. 3381–3385.

[25] O. De Candido, H. Jedda, A. Mezghani, A. L. Swindlehurst, and J. A. Nossek, "Reconsidering linear transmit signal processing in 1-bit quantized multi-user MISO systems," *IEEE Trans. Wireless Commun.*, vol. 18, no. 1, pp. 254–267, 2019.

[26] Y. Li, C. Tao, A. Mezghani, A. L. Swindlehurst, G. Seco-Granados, and L. Liu, "Optimal design of energy and spectral efficiency tradeoff in one-bit massive MIMO systems." [Online]. Available: https://arxiv.org/abs/1612.03271

[27] A. K. Saxena, A. Mezghani, and R. W. Heath, "Linear CE and 1-bit quantized precoding with optimized dithering," *IEEE Open J. of Signal Process.*, vol. 1, pp. 310–325, 2020.

[28] H. Jedda, J. A. Nossek, and A. Mezghani, "Minimum BER precoding in 1-bit massive MIMO systems," in *2016 IEEE Sensor Array and Multichannel Signal Process. Workshop (SAM)*, 2016, pp. 1–5.

[29] H. Jedda, A. Mezghani, A. L. Swindlehurst, and J. A. Nossek, "Quantized constant envelope precoding with PSK and QAM signaling," *IEEE Trans. on Wireless Commun.*, vol. 17, no. 12, pp. 8022–8034, 2018.

[30] O. Castañeda, T. Goldstein, and C. Studer, "POKEMON: A non-linear beamforming algorithm for 1-bit massive MIMO," in *2017 IEEE Int. Conf. on Acoust., Speech and Signal Process. (ICASSP)*, 2017, pp. 3464–3468.

[31] S. Jacobsson, G. Durisi, M. Coldrey, and C. Studer, "On out-of-band emissions of quantized precoding in massive MU-MIMO-OFDM," in *2017 51st Asilomar Conf. on Signals, Syst., and Comput.*, 2017, pp. 21–26.

[32] T. Yamakado, R. Okawa, and Y. Sanada, "Quantized precoding for out-of-band radiation reduction in massive MU-MIMO-OFDM," in *2021 IEEE 94th Veh. Technol. Conf. (VTC2021-Fall)*, 2021, pp. 1–5.

[33] O. Özdogan, E. Björnson, and E. G. Larsson, "Massive MIMO with spatially correlated Rician fading channels," *IEEE Trans. on Commun.*, vol. 67, no. 5, pp. 3234–3250, 2019.

[34] A. Kurt and G. M. Guvensen, "An adaptive hybrid beamforming scheme for time-varying wideband massive MIMO channels," in *ICC 2020 - 2020 IEEE Int. Conf. on Commun. (ICC)*, 2020, pp. 1–7.

[35] O. T. Demir and E. Bjornson, "The Bussgang decomposition of nonlinear systems: Basic theory and MIMO extensions [lecture notes]," *IEEE Signal Process. Mag.*, vol. 38, no. 1, pp. 131–136, 2021.

[36] A. B. Üçüncü, E. Björnson, H. Johansson, A. Ö. Yılmaz, and E. G. Larsson, "Performance analysis of quantized uplink massive MIMO-OFDM with over-

sampling under adjacent channel interference," *IEEE Trans. Commun.*, vol. 68, no. 2, pp. 871–886, Feb. 2020.

[37] J. Van Vleck and D. Middleton, "The spectrum of clipped noise," *Proceedings of the IEEE*, vol. 54, no. 1, pp. 2–19, 1966.

[38] M. Salehi and J. Proakis, *Digital Communications*. New York, NY, USA: McGraw-Hill, 2007.

[39] *IEEE Draft Standard for Information Technology – Telecommunications and Information Exchange Between Systems Local and Metropolitan Area Networks – Specific Requirements - Part 11: Wireless LAN Medium Access Control (MAC) and Physical Layer (PHY) Specifications*, Std. IEEE P802.11-REVmd/D1.0, Feb. 2018.

[40] Y. Karabacakoğlu, A. B. Üçüncü, and G. M. Guvensen, "An iterative distortion-aware precoding for quantized upsampled wideband massive MIMO," *presented at 2023 IEEE Int. Conf. Commun. (ICC), Rome, Italy*, May 28- Jun. 1, 2023.

Appendix A

PROOFS IN CHAPTER 4

A.1 Proof of Proposition 1

r_k^u can be found from f_k^u as

$$X_d(e^{j\frac{2\pi k}{\mu K}}) \triangleq r_k^u, \quad X(e^{j\frac{2\pi k}{\mu_c K}}) \triangleq f_k^u, \tag{A.1}$$

$$X_d(e^{jw}) = \frac{1}{M}\sum_{m=0}^{M-1} X(e^{j(\frac{w-2\pi m}{M})}),\ w = \frac{2\pi k}{\mu K} \tag{A.2}$$

$$X_d(e^{j\frac{2\pi k}{\mu K}}) = \frac{1}{M}\sum_{m=0}^{M-1} X(e^{j(\frac{2\pi k}{M\mu K}-\frac{2\pi m}{M})}),\ M = \mu_c/\mu \tag{A.3}$$

$$X_d(e^{j\frac{2\pi k}{\mu K}}) = \frac{\mu}{\mu_c}\sum_{m=0}^{\mu_c/\mu-1} X(e^{j(\frac{2\pi k\mu}{\mu_c\mu K}-\frac{2\pi m\mu K}{\mu_c K})}) \tag{A.4}$$

$$r_k = \frac{\mu}{\mu_c}\sum_{m=0}^{\mu_c/\mu-1} X(e^{j\frac{2\pi}{\mu_c K}(k-m\mu K)}) = \frac{\mu}{\mu_c}\sum_{m=0}^{\mu_c/\mu-1} f_{(k-m\mu K)_{\mu_c K}}, \tag{A.5}$$

Here (A.2) hold by definition. Change of variables, namely ($w = \frac{2\pi k}{\mu K}$) and ($M = \mu_c/\mu$) is introduced in (A.2) and (A.3), respectively.

A.2 Proof of Proposition 2

$\mathbf{C}_{\boldsymbol{\eta}_k}$ can be found from $\mathbf{C}_{\tilde{\boldsymbol{\eta}}}[m]$ as

$$\mathbf{C}_{\boldsymbol{\eta}_k} = E\left[\boldsymbol{\eta}_k(\boldsymbol{\eta}_k)^H\right] \tag{A.6}$$

$$= \frac{1}{\mu K}\sum_{n=0}^{\mu K-1}\sum_{n'=0}^{\mu K-1} E\left[\widetilde{\boldsymbol{\eta}}_n(\widetilde{\boldsymbol{\eta}}_{n'})^H\right] e^{\frac{-j2\pi nk}{\mu K}} e^{\frac{j2\pi n'k}{\mu K}} \tag{A.7}$$

$$= \frac{1}{\mu K}\sum_{n=0}^{\mu K-1}\sum_{n'=0}^{\mu K-1} \mathbf{C}_{\widetilde{\boldsymbol{\eta}}}[n-n'] e^{\frac{-j2\pi(n-n')k}{\mu K}} \tag{A.8}$$

$$= \frac{1}{\mu K}\sum_{m=-(\mu K-1)}^{\mu K-1} (\mu K - |m|)\mathbf{C}_{\widetilde{\boldsymbol{\eta}}}[m] e^{\frac{-j2\pi(m)k}{\mu K}} \tag{A.9}$$

$$= \frac{1}{\mu K}\sum_{m=0}^{\mu K-1} (\mu K - m)\mathbf{C}_{\widetilde{\boldsymbol{\eta}}}[m] e^{\frac{-j2\pi(m)k}{\mu K}}$$

$$+ \frac{1}{\mu K}\sum_{m=0}^{\mu K-1} (\mu K - m)(\mathbf{C}_{\widetilde{\boldsymbol{\eta}}}[m])^H e^{\frac{j2\pi(m)k}{\mu K}} - \mathbf{C}_{\widetilde{\boldsymbol{\eta}}}[0] \tag{A.10}$$

$$= \boldsymbol{\Gamma}_k + \boldsymbol{\Gamma}_k^H - \mathbf{C}_{\widetilde{\boldsymbol{\eta}}}[0] \tag{A.11}$$

Here (A.7)-(A.8) directly comes from definition and stationarity of $\widetilde{\boldsymbol{\eta}}_n$. (A.9) is by change of variable ($m = n - n'$). (A.10) holds because $(\mathbf{C}_{\widetilde{\boldsymbol{\eta}}}[m])^H = \mathbf{C}_{\widetilde{\boldsymbol{\eta}}}[-m]$.

A.3 Proof of Proposition 3

$\mathbf{C}_{\widetilde{\mathbf{x}}}[m]$ can be found from $\mathbf{C}_{\mathbf{x}_k}$ as

$$\mathbf{C}_{\widetilde{\mathbf{x}}}[m] = E\left[\widetilde{\mathbf{x}}_n\widetilde{\mathbf{x}}_{n-m}^H\right] \tag{A.12}$$

$$= \frac{1}{\mu K}\sum_{k=0}^{\mu K-1}\sum_{k'=0}^{\mu K-1} E\left[\mathbf{x}_k(\mathbf{x}_{k'})^H\right] e^{\frac{j2\pi nk}{\mu K}} e^{\frac{-j2\pi(n-m)k'}{\mu K}} \tag{A.13}$$

$$= \frac{1}{\mu K}\sum_{k=0}^{\mu K-1} E\left[\mathbf{x}_k(\mathbf{x}_k)^H\right] e^{\frac{j2\pi nk}{\mu K}} e^{\frac{-j2\pi(n-m)k}{\mu K}} \tag{A.14}$$

$$= \frac{1}{\mu K}\sum_{k=0}^{\mu K-1} \mathbf{C}_{\mathbf{x}_k} e^{\frac{j2\pi mk}{\mu K}} \tag{A.15}$$

Here (A.13) holds by definition, (A.14) is valid since $E\left[\mathbf{x}_k(\mathbf{x}_k)^H\right] = \mathbf{0}_{Nt\times Nt}$, for $k \neq k'$ as the message signal in frequency domain is uncorrelated. (A.15) is by definition.